Analysis of different resolution methods for planing hulls

NepTech
Intelligent sea mobility

Version	Date	Written by	Validated by
1	31/03/2025	Tanguy TEULET	Clément ROUSSET

Table of contents

Summary

This report presents a comprehensive study on the influence of meshing strategies and numerical parameters on the accuracy and efficiency of CFD simulations for planning hulls, using NepTech's digital testing basin. The study focuses on a high-speed regime, covering a Froude number range from 1.2 to 2.7, based on GPPH. The analysis compares four different approaches, showing that the most accurate setup provides highly precise results, while a faster alternative allows for efficient design exploration with a slight trade-off in accuracy. The study also demonstrates significant reductions in computation time, up to 4.9 times faster. These developments reinforce the adaptability and efficiency of NepTech's digital testing basin for high-fidelity CFD simulations tailored to various project requirements.

Nomenclature

- F_n $[-]$, Froude number.
- CFD, Computational Fluid Dynamic.
- EFD, Experimental Fluid Dynamic.
- LCG ; TCG ; VCG $[m]$, coordinates of the centre of gravity: lateral, transversal and vertical.
- V $[m/s]$, ship speed.
- μ $[Pa.s]$, dynamic viscosity.
- ρ $[kg/m^3]$, density.

Figures

Tables

1. Introduction

Planing hulls pose significant computational challenges due to their complex hydrodynamic behaviour, often resulting in long simulation times in CFD analyses. Optimizing the resolution strategy is therefore essential to reducing computational costs while maintaining accuracy.

This study explores different approaches to improving the efficiency of planing hull simulations by analysing both meshing techniques and simulation assumptions. The impact of these factors on computational performance and accuracy is evaluated to identify the most effective strategies.

Since the core simulation parameters remain identical across all methods, this study focuses primarily on assessing the influence of meshing approaches and modelling assumptions. Detailed simulation settings are not discussed here, as they are already covered in a dedicated CFD/EFD comparative report available on the NepTech website. Additionally, the validation of meshing techniques (overset mesh and mesh deformation) is addressed in a separate report available on the same platform.

This paper provides valuable insights into the impact of different meshing and modelling strategies, helping to identify the most efficient and reliable approach for planing hull simulations.

2. GPPH

The Generatic Prismatic Planing Hull (GPPH) hull was designed as a publicly available reference model to support research and development across government agencies, contractors, and academic institutions. Its prismatic design was specifically chosen to represent typical planning hulls while minimizing geometric complexities such as warp, rocker, and curvature in both transverse and longitudinal directions.

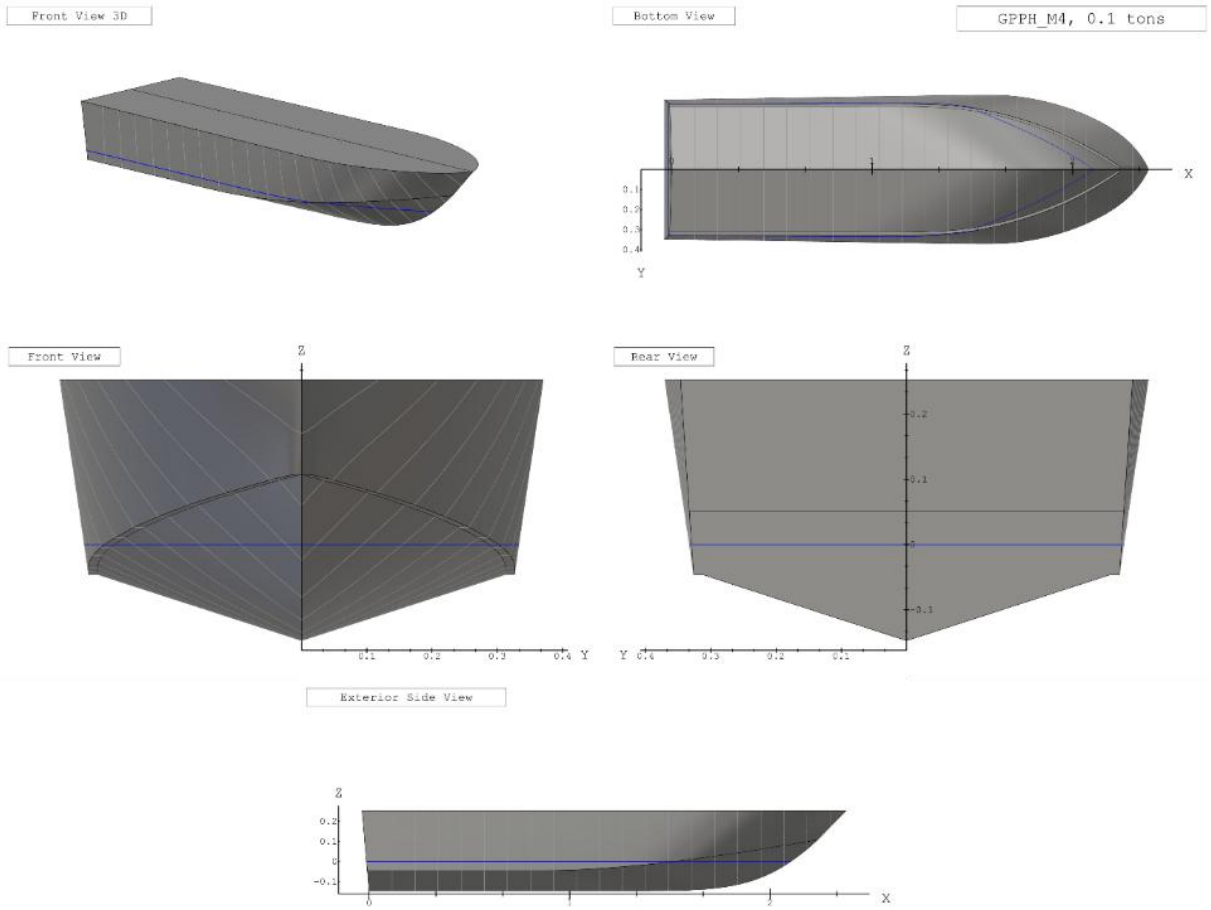

Figure 1: GPPH CAD model

3. Resolution strategies

This section details the four resolution strategies analysed in this study. Each method differs in terms of meshing approach and initial simulation assumptions, impacting both computational efficiency and accuracy.

- M1: Overset mesh with a pre-estimated initial pitch angle and an acceleration ramp.
- M2: Mesh deformation with a pre-estimated initial pitch angle, and an acceleration ramp.
- M3: Mesh deformation with both a pre-estimated initial pitch angle and sinkage, along with an acceleration ramp.
- M4: Mesh deformation with both a pre-estimated initial pitch angle and sinkage, without an acceleration ramp.

In this study, the pre-estimated trim and sinkage values are based on experimental results from Lee, E., Weil, R., & Fullerton, A. (2017). *Experimental Results for the Calm Water Resistance of the Generic Prismatic Planing Hull (GPPH)*. These results, obtained from towing tank experiments, serve as a reliable reference for setting initial conditions in our simulations.

However, in a more general context where experimental data is unavailable, pre-estimated trim and sinkage values can be derived from a database of existing results or estimated using empirical methods such as Savitsky's method. This flexibility allows for adapting the approach to different planning hull configurations and available data sources.

4. Validation

a. Mesh

Hull: The accuracy of the results regarding viscous resistance mainly depends on the mesh of the hull. This resistance is caused by the entrainment of a thin fluid film: the boundary layer. An appropriate mesh of the boundary layer is essential to correctly capture local phenomena such as viscous effects and rapid variations in fluid properties near the surface. It also allows for better capture and resolution of turbulent phenomena if they are present. The quality of the hull mesh also affects the fidelity of the 3D model representation. A clean and regular mesh improves the reliability of the simulation, making the simulated model more representative of the actual vessel.

Figure 9 to Figure 15 illustrates the hull mesh configurations used for the various speeds and for all methods considered in the study.

Free surface: The accuracy of the results regarding pressure resistance mainly depends on how the air-water interface is captured during simulation. This resistance is induced by the wave field generated by the vessel, and the quality of the mesh for the latter plays a crucial role in this accuracy. The use of AGR allows dynamically adapting the mesh based on the generated wave field, achieving maximum precision, as it is one of the most advanced and reliable methods to date and reducing computation time by converging more quickly toward the dynamic equilibrium state.

Figure 16 to Figure 22 illustrates the free surface mesh configurations used for the various speeds and for all methods considered in the study.

Values:

Ship speed $\mathbf{V}$ [knots]		10.80	13.00	14.80	17.50	19.50	21.60	23.80
Froude number $\mathbf{F_n}$ [−]		1.22	1.47	1.67	1.98	2.20	2.44	2.69
Averaged number of cells [*10^6]	M1	3.50	3.24	3.18	3.04	3.11	3.06	3.01
	M2	1.65	1.61	1.67	1.65	1.72	1.73	1.73
	M3	1.64	1.60	1.65	1.63	1.70	1.71	1.70
	M4	1.62	1.58	1.63	1.59	1.65	1.66	1.66

Table 1: Averaged number of cells

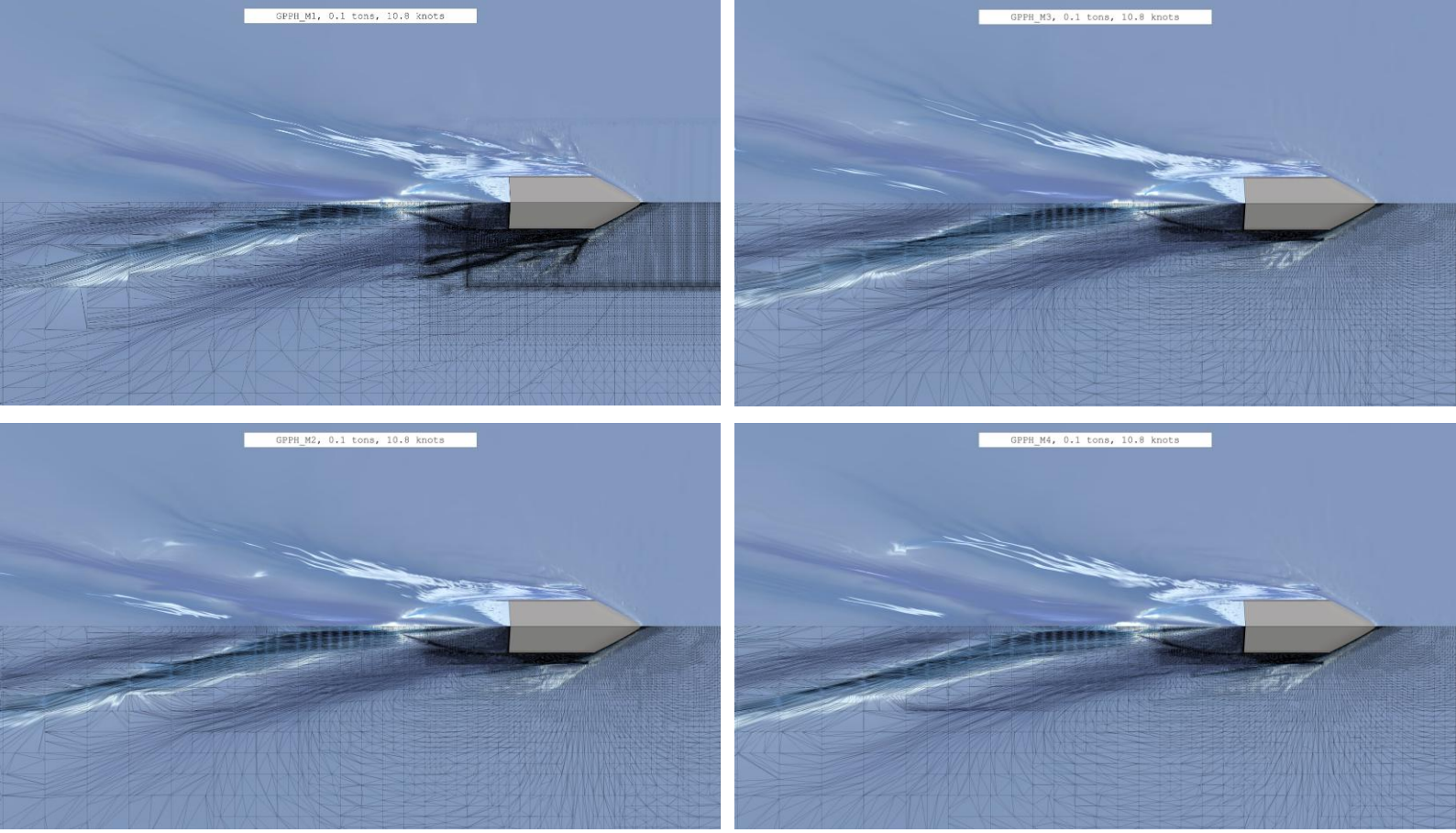

Figure 2: Free surface mesh at 10.80 knots

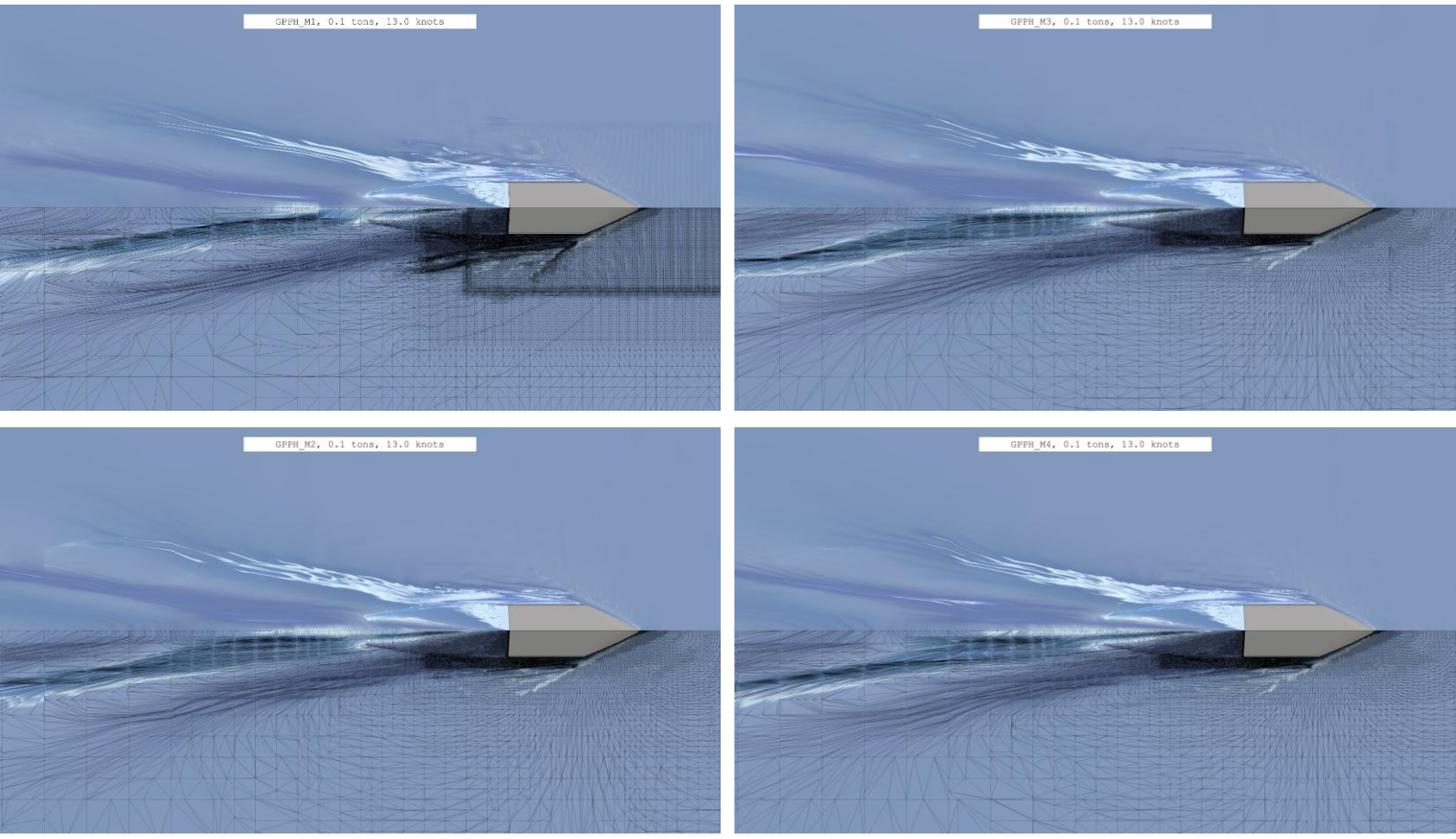

Figure 3: Free surface mesh at 13.00 knots

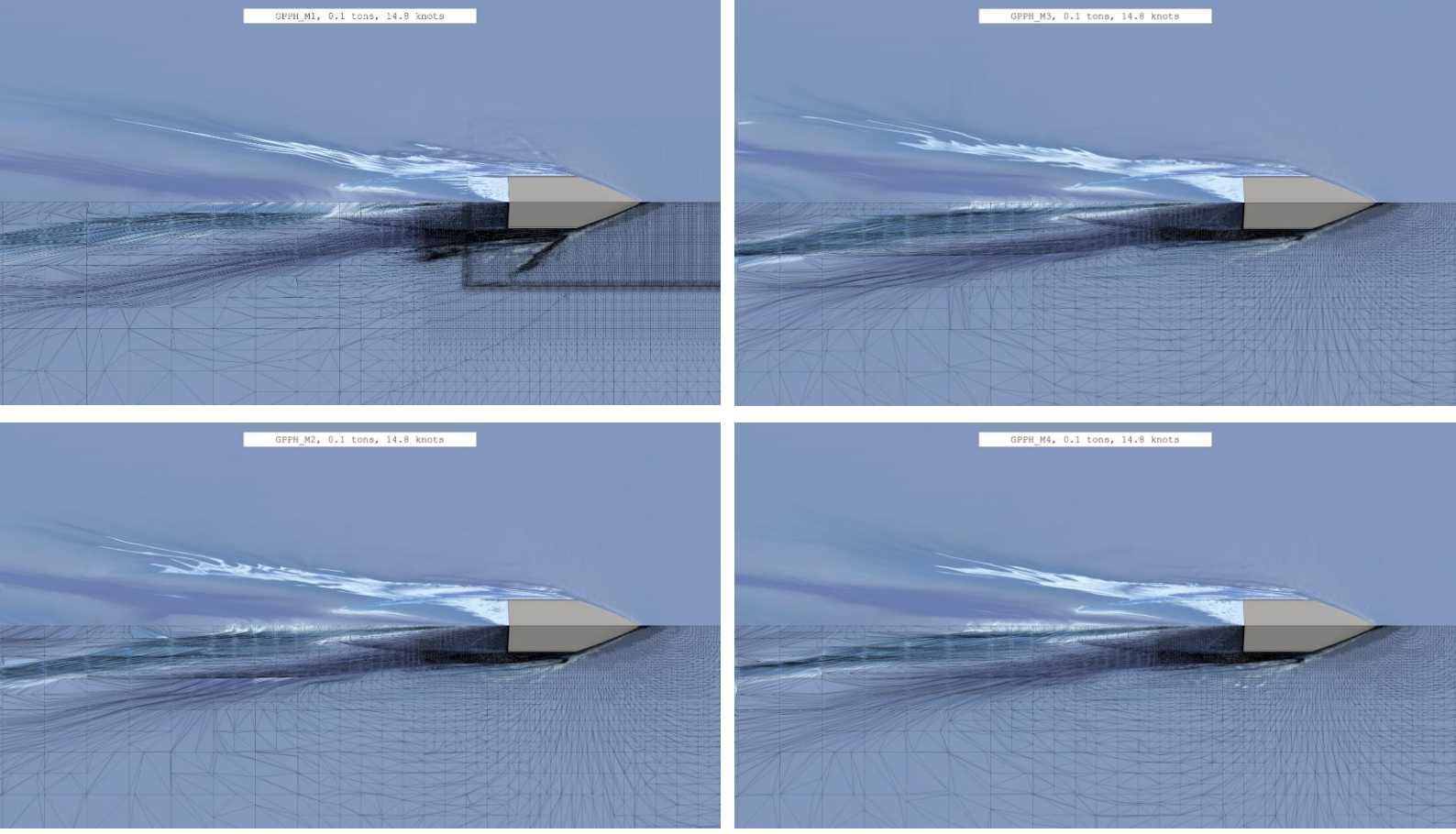

Figure 4: Free surface mesh at 14.80 knots

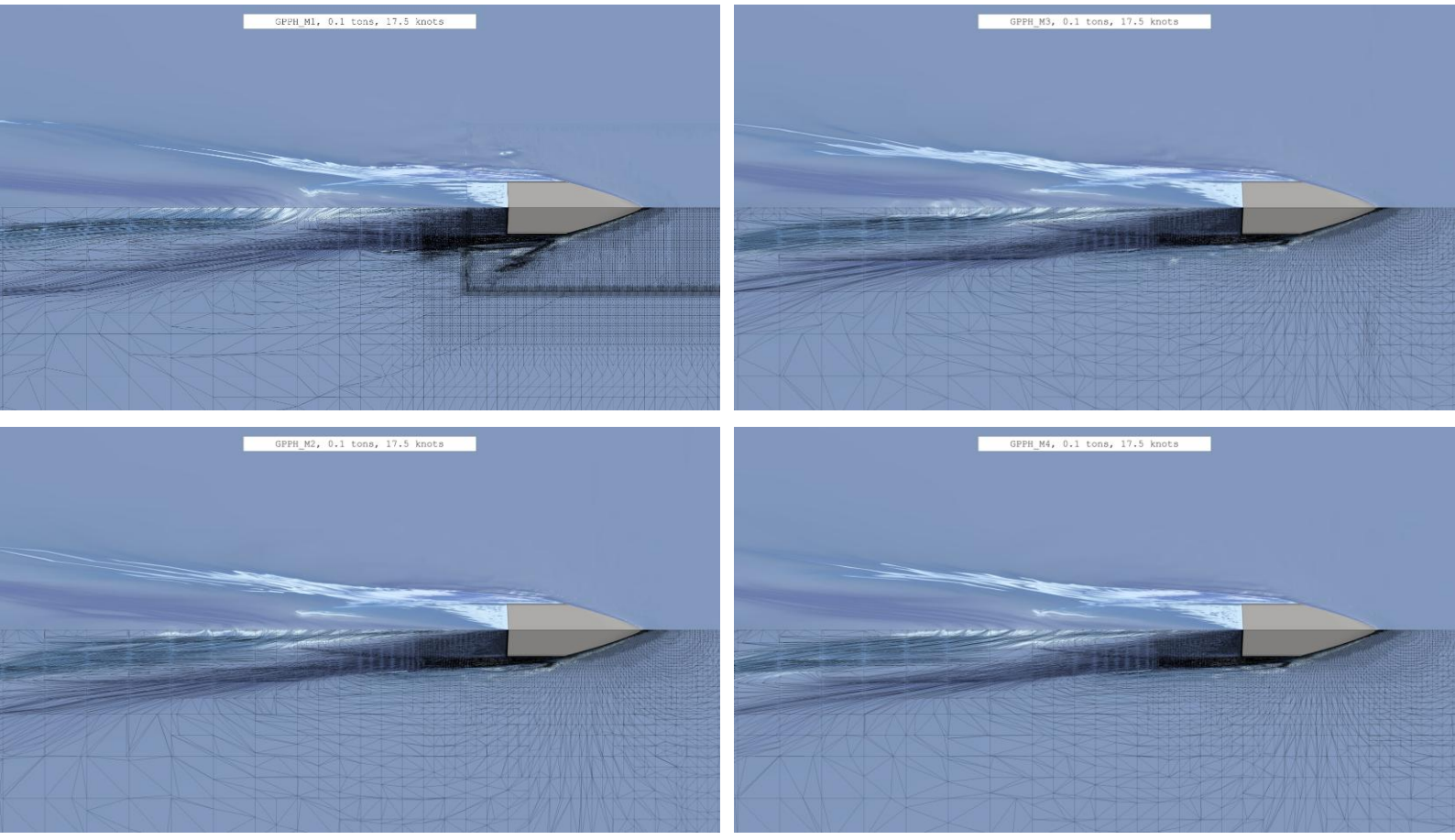

Figure 5: Free surface mesh at 17.50 knots

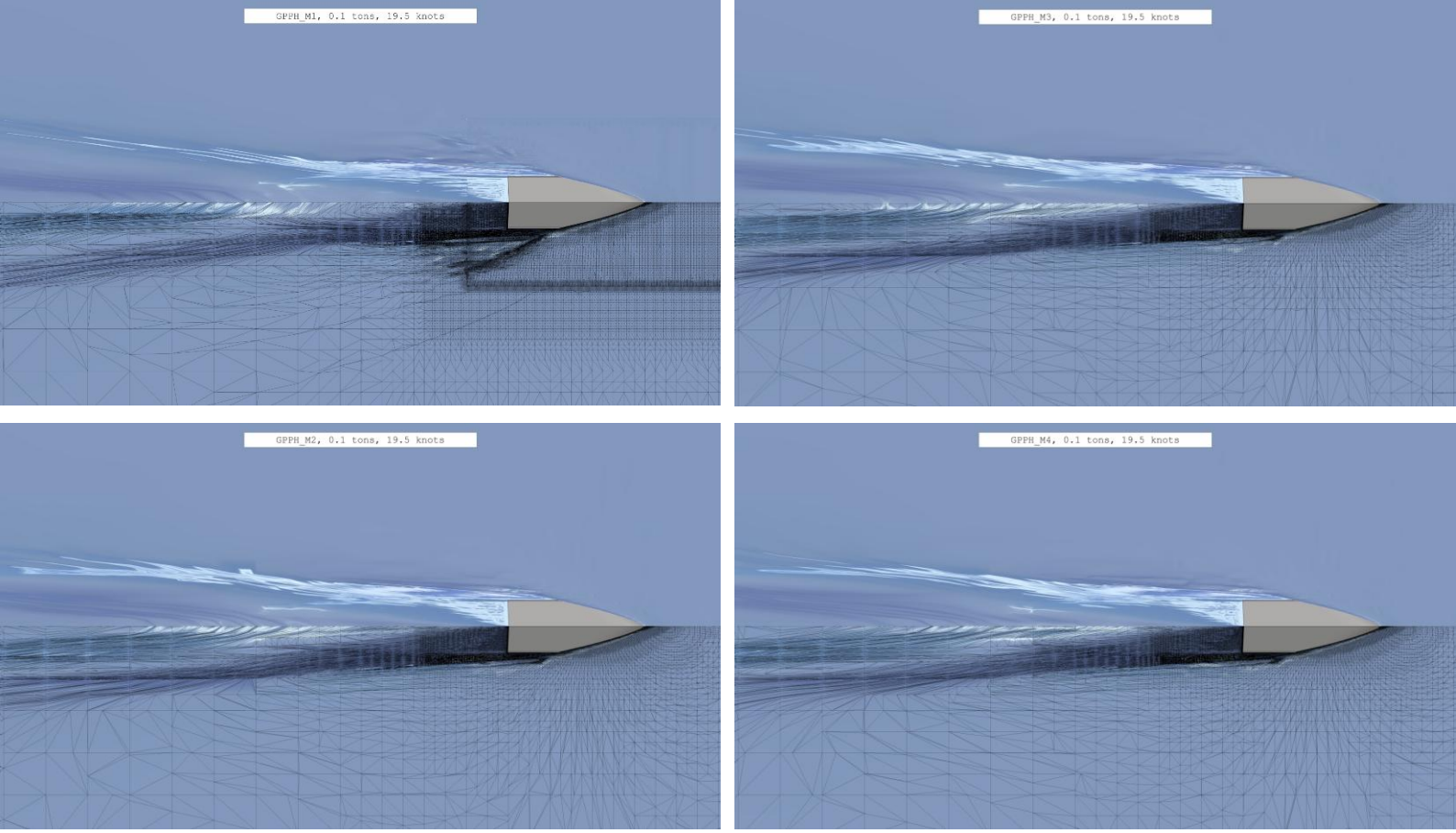

Figure 6: Free surface mesh at 19.50 knots

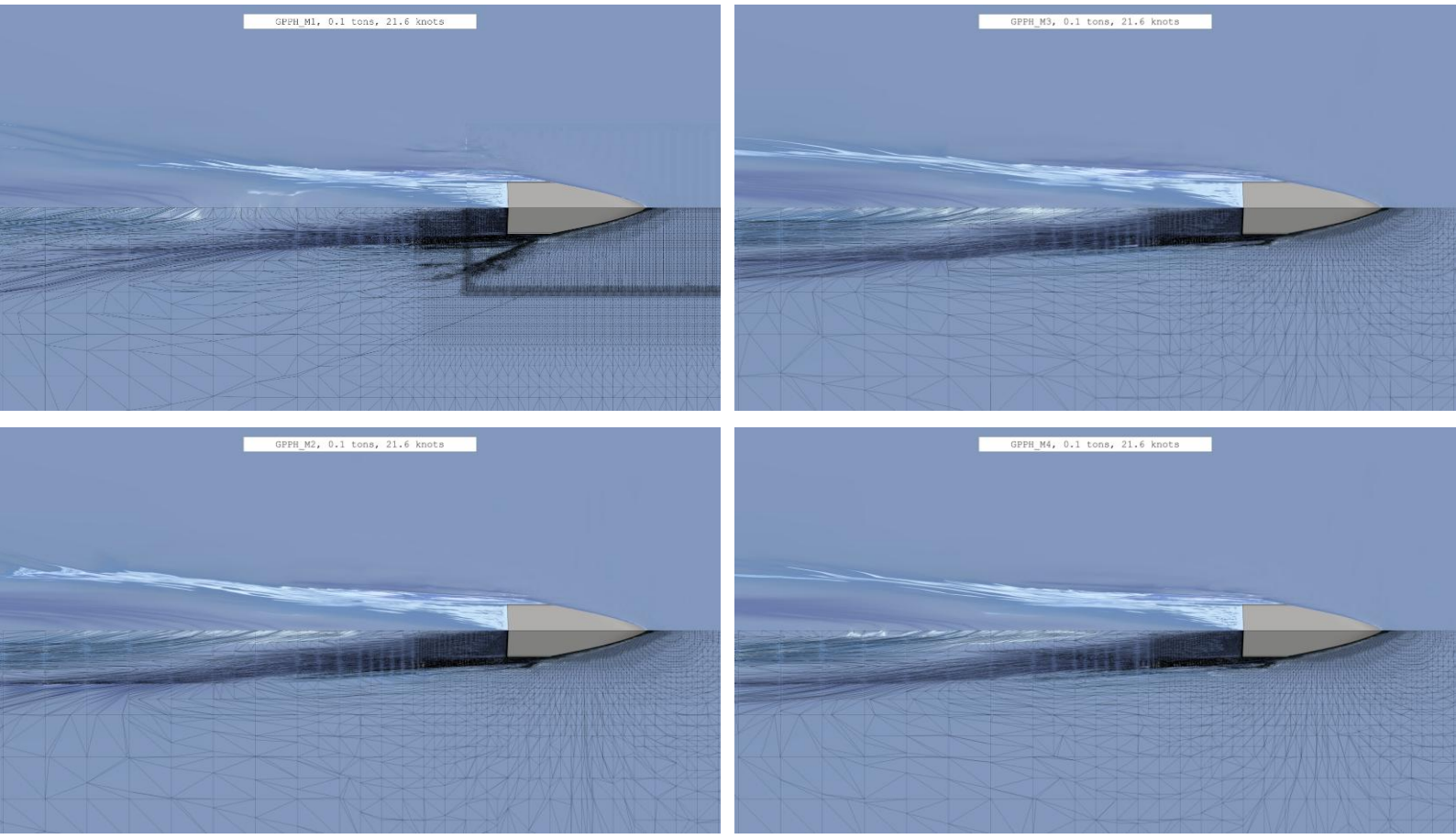

Figure 7: Free surface mesh at 21.60 knots

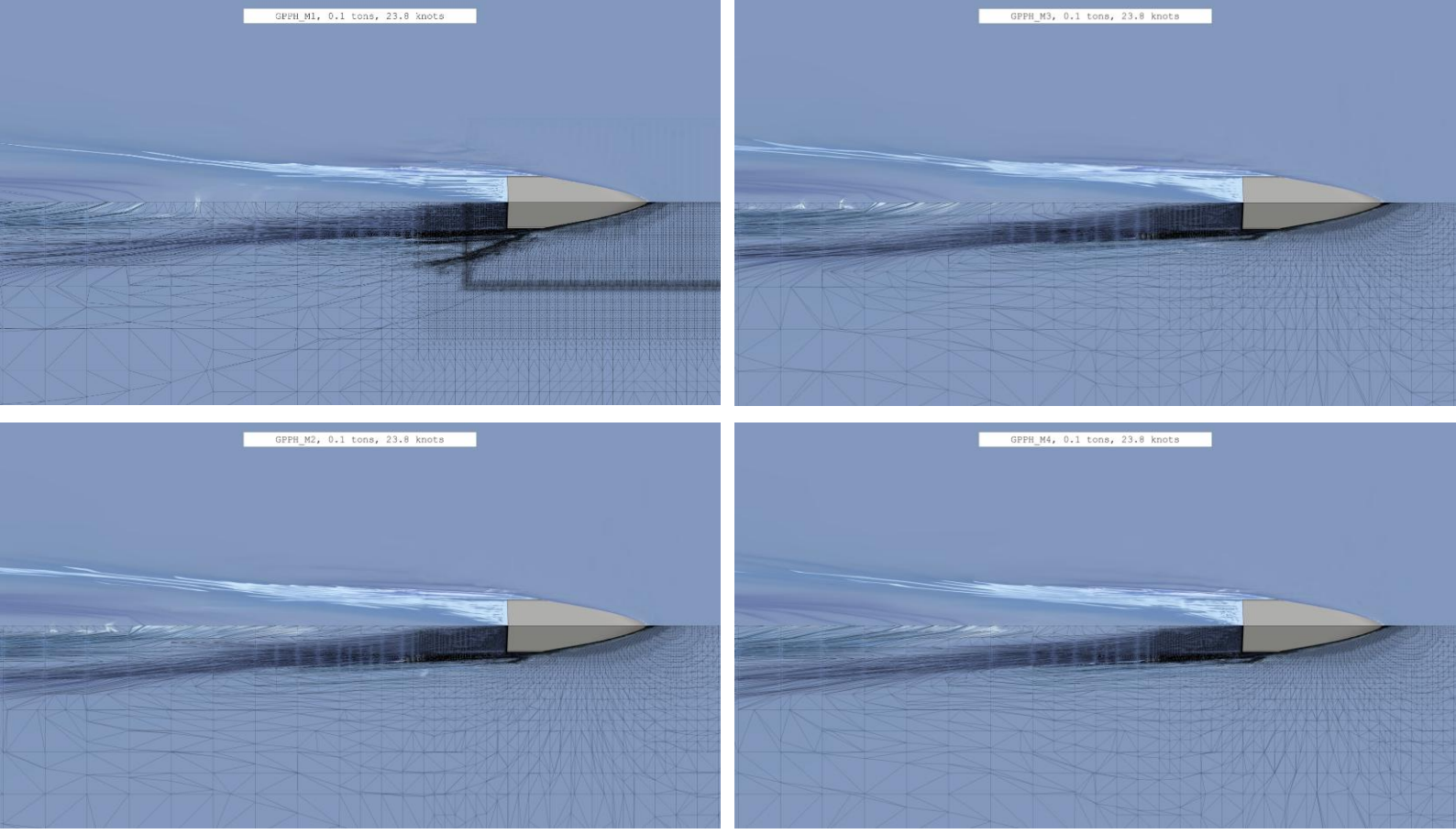

Figure 8: Free surface mesh at 23.80 knots

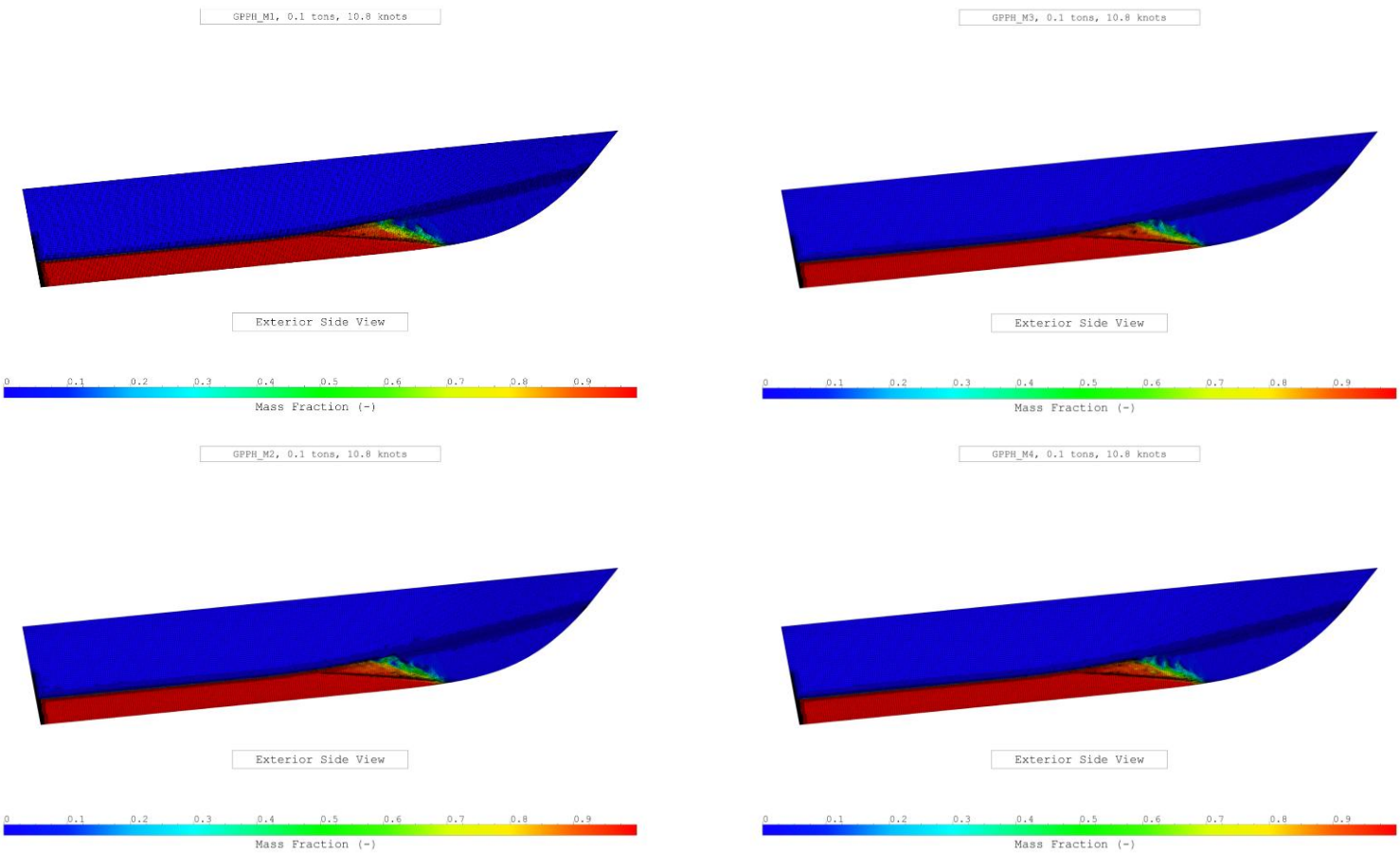

Figure 9: Bare hull mesh at 10.80 knots

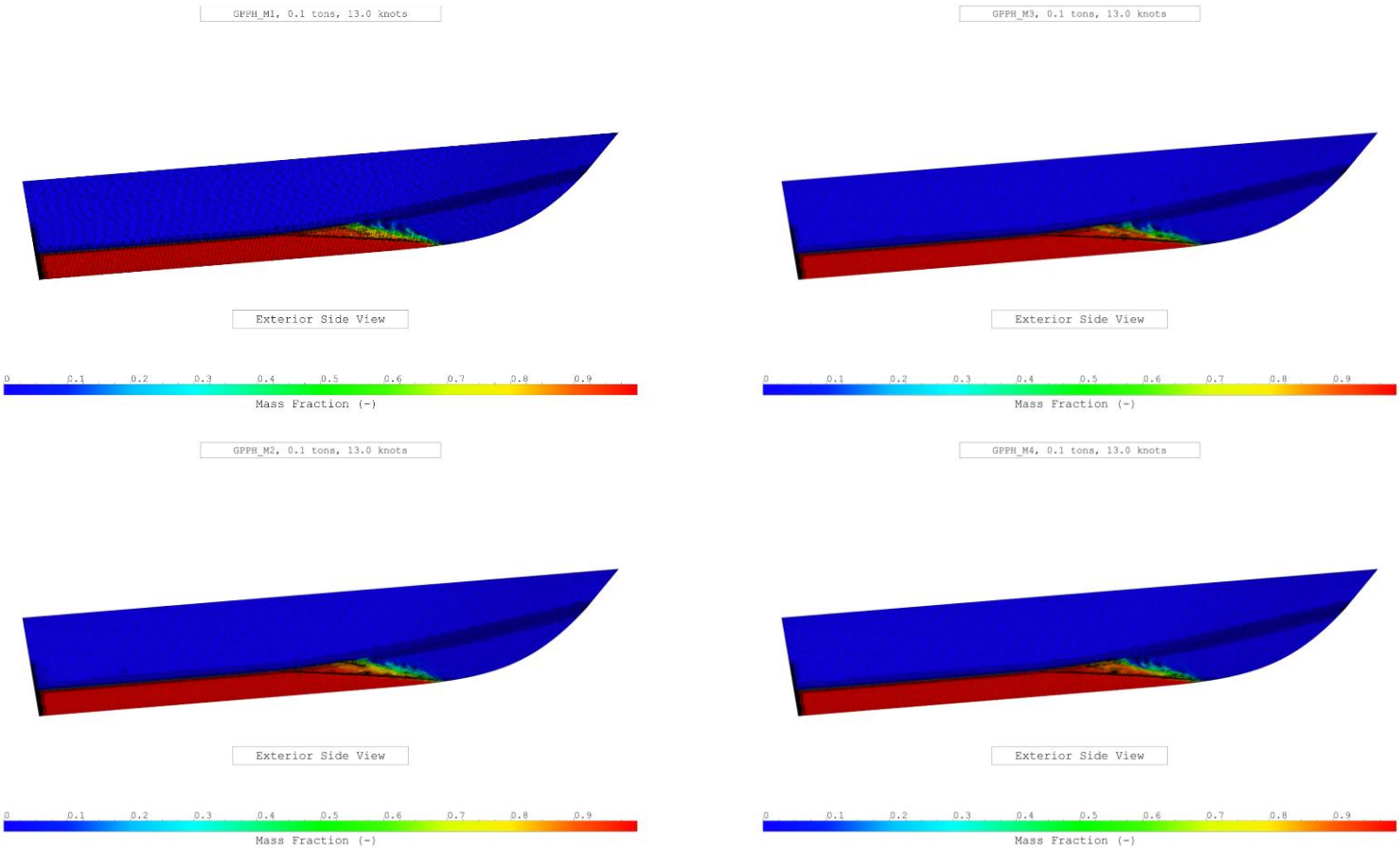

Figure 10: Bare hull mesh at 13.00 knots

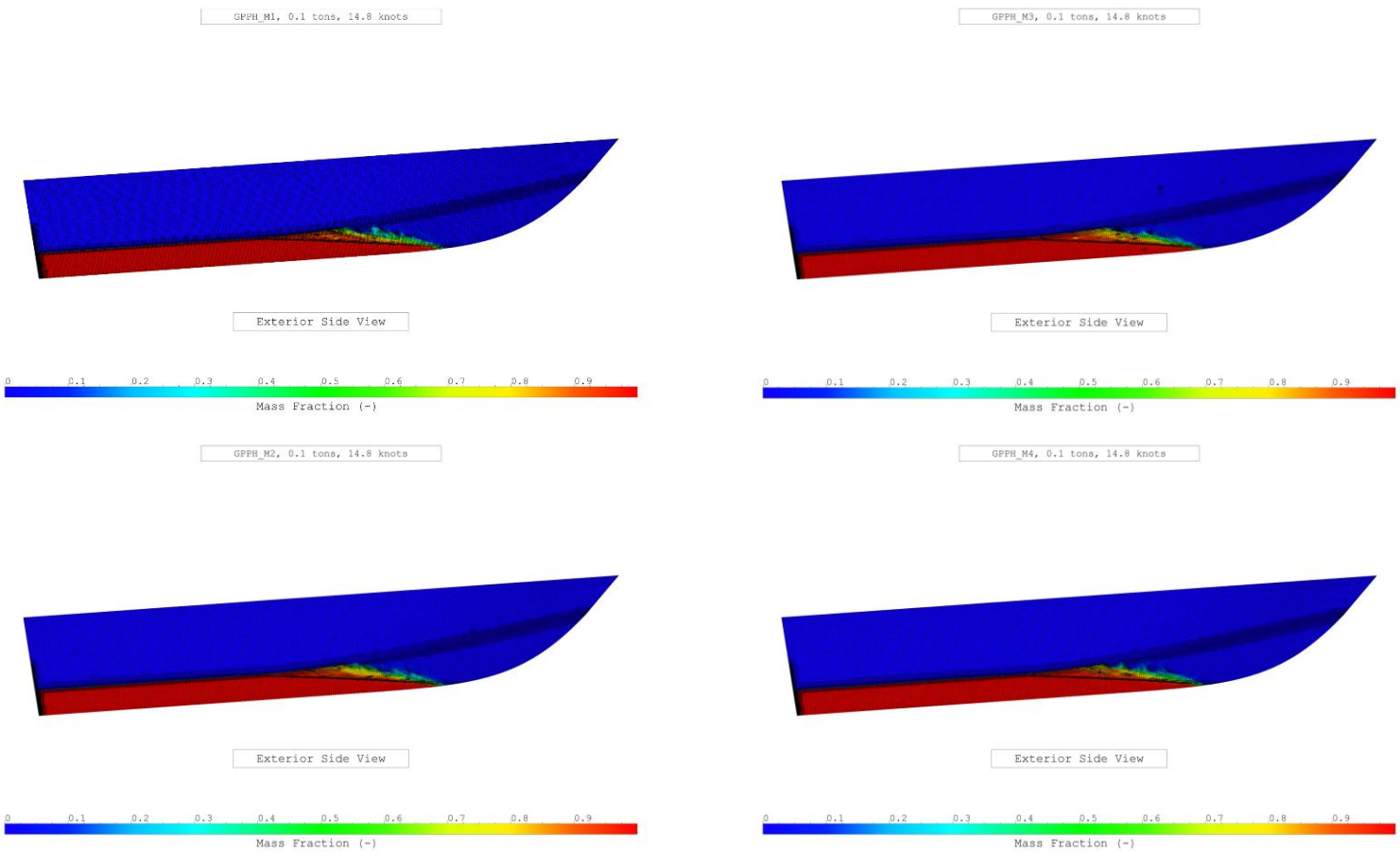

Figure 11: Bare hull mesh at 14.80 knots

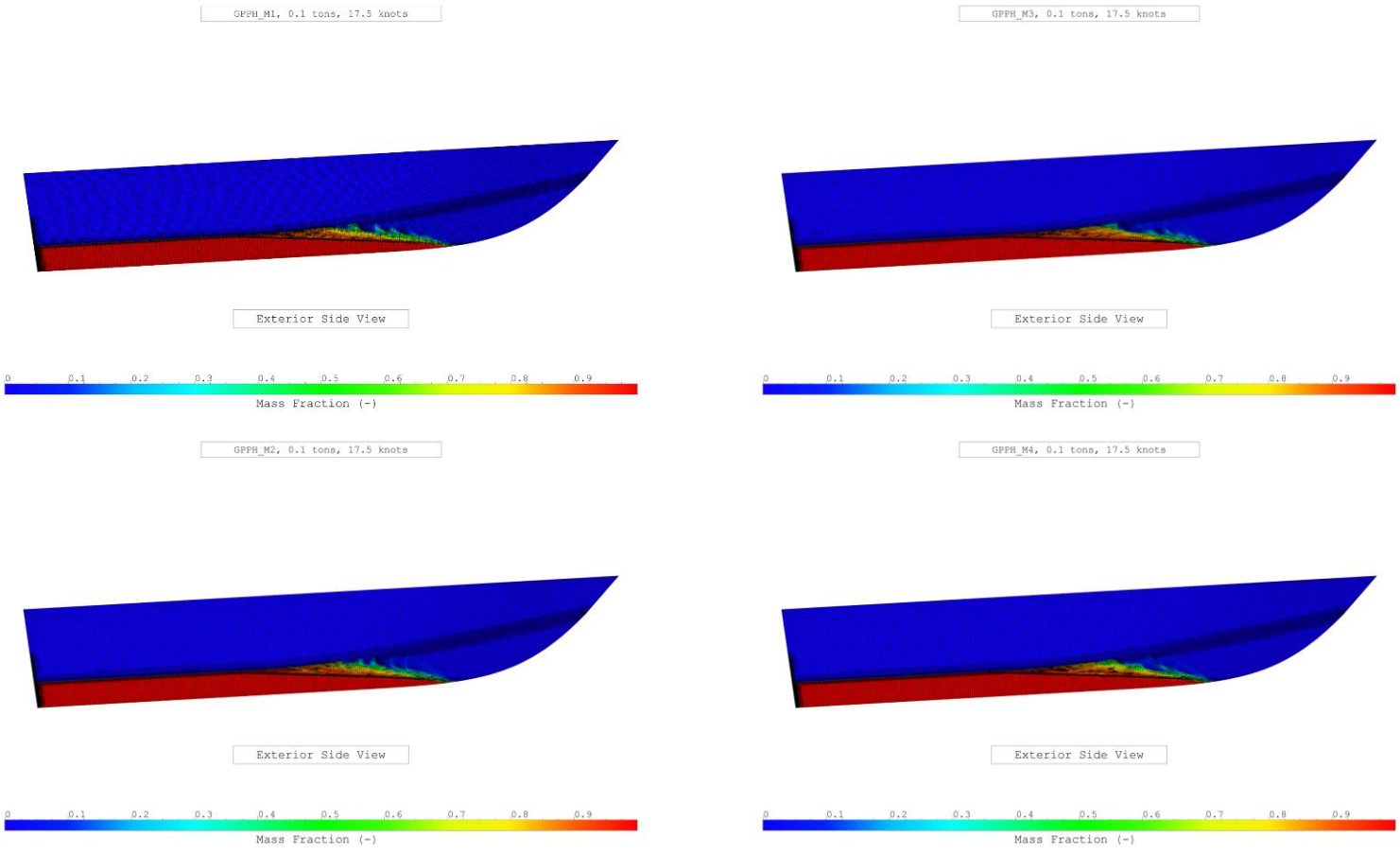

Figure 12: Bare hull mesh at 17.50 knots

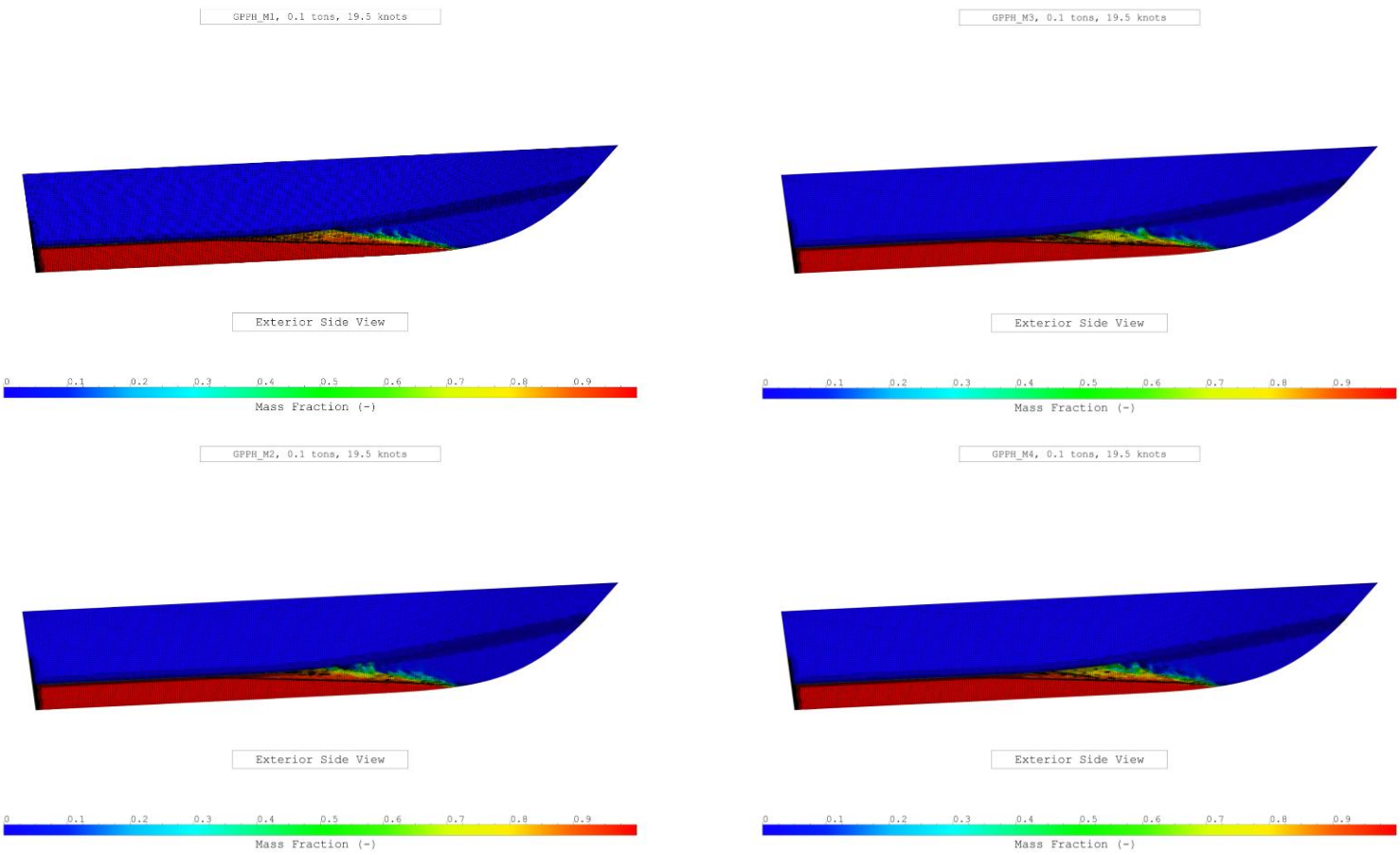

Figure 13: Bare hull mesh at 19.50 knots

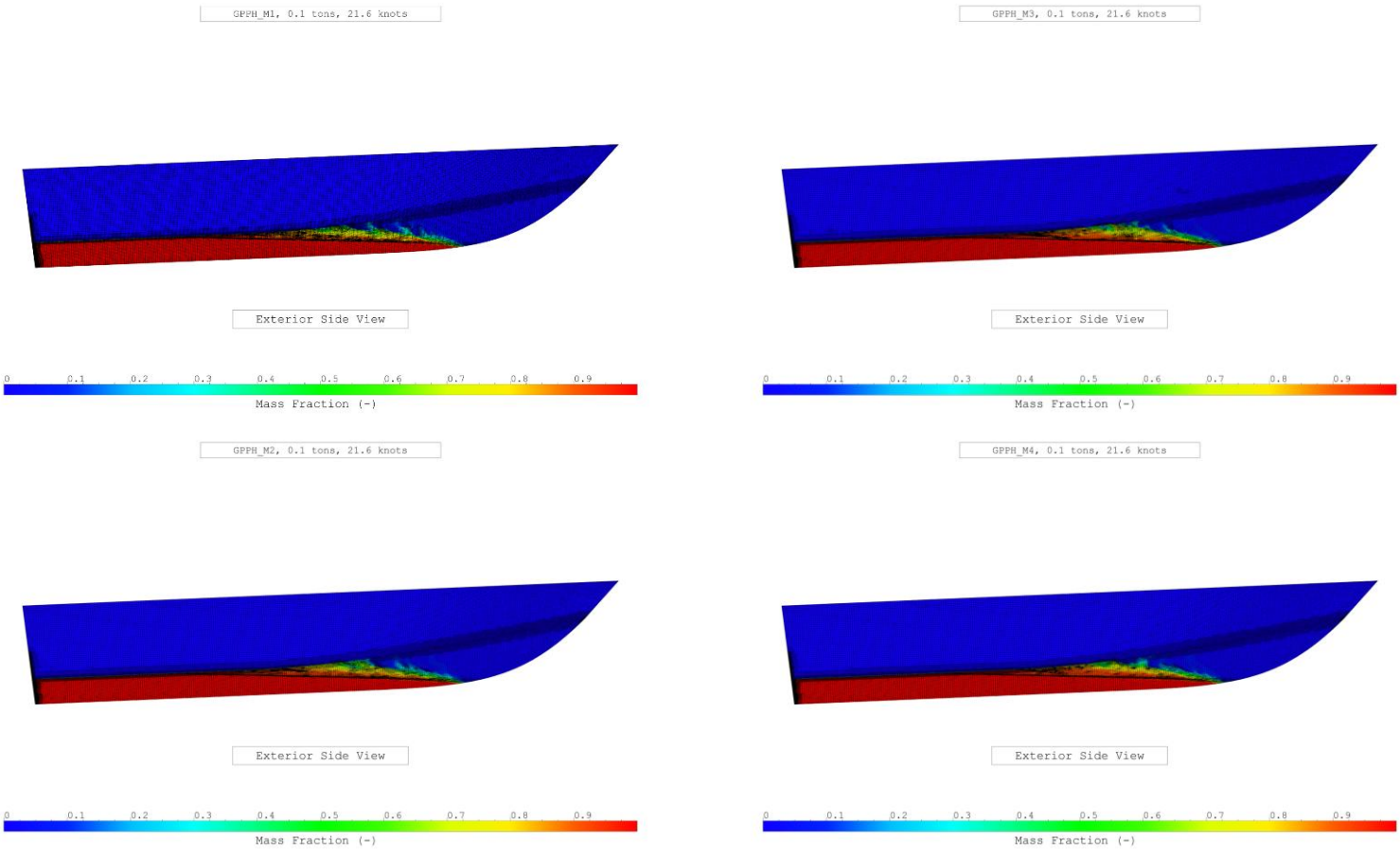

Figure 14: Bare hull mesh at 21.60 knots

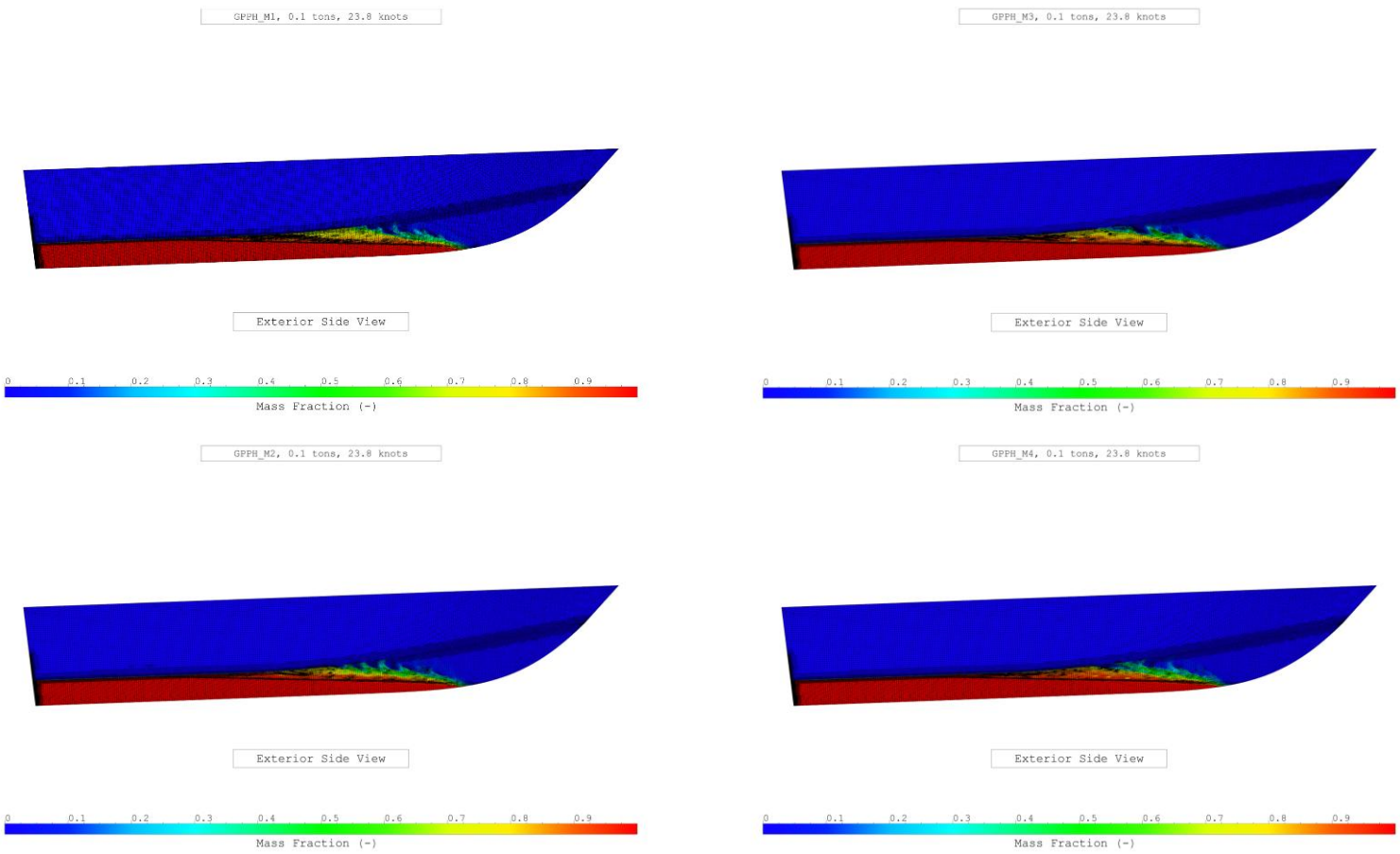

Figure 15: Bare hull mesh at 23.80 knots

b. Courant number

Description: The Courant number, also called the CFL (Courant-Friedrichs-Lewy) number, is a crucial parameter in computational fluid dynamics (CFD). It measures the numerical stability of the discretization scheme used in the simulation. An inappropriate Courant number can lead to numerical instabilities, compromising both convergence and the accuracy of the results. In CFD, the Courant number is related to the size of the numerical time steps. It is calculated by comparing the speed of fluid particles with the size of the cells in the simulation domain.

Recommended values: For typical resistance simulations, it is recommended to keep the Courant number below or close to 1 to ensure maximum accuracy and reliability. Local spikes in this parameter may occur, but it is essential to control them to maintain numerical stability and the quality of the results.

Values:

Ship speed $\mathbf{V}$ [knots]		10.80	13.00	14.80	17.50	19.50	21.60	23.80
Froude number $\mathbf{F_n}$ [−]		1.22	1.47	1.67	1.98	2.20	2.44	2.69
Averaged Courant number [-]	M1	0.24	0.21	0.18	0.15	0.15	0.14	0.13
	M2	0.19	0.16	0.13	0.11	0.10	0.10	0.09
	M3	0.19	0.16	0.13	0.11	0.10	0.10	0.09
	M4	0.18	0.16	0.13	0.11	0.10	0.10	0.09

Table 2: Averaged Courant number (Free Surface)

Ship speed $\mathbf{V}$ [knots]		10.80	13.00	14.80	17.50	19.50	21.60	23.80
Froude number $\mathbf{F_n}$ [−]		1.22	1.47	1.67	1.98	2.20	2.44	2.69
Averaged Courant number [-]	M1	1.33	1.31	1.32	1.29	1.30	1.30	1.32
	M2	1.35	1.34	1.34	1.33	1.30	1.31	1.29
	M3	1.35	1.34	1.33	1.32	1.33	1.32	1.32
	M4	1.36	1.34	1.34	1.33	1.31	1.30	1.28

Table 3: Averaged Courant number (Hull)

c. Y+

Description: In the naval field, managing the Y+ parameter is crucial in computational fluid dynamics (CFD) simulations. Y+ measures the quality of the boundary layer resolution along the submerged surfaces of ship hulls by evaluating the distance between the first mesh point and the wall relative to the boundary layer thickness. Maintaining an appropriate Y+ is essential to ensure reliable results in predicting resistance, drag, lift, and other critical hydrodynamic phenomena. An improper Y+ can lead to significant errors in the prediction of forces, drag coefficients, and other key parameters.

Recommended values: For typical resistance simulations, it is recommended that the Y+ value be between 30 and 300. This value may be lower depending on the choice of boundary layer modeling. Local spikes in this parameter may occur, but it is essential to control them to maintain numerical stability and the quality of the results.

Values:

Ship speed $\mathbf{V}$ $[\mathbf{knots}]$		10.80	13.00	14.80	17.50	19.50	21.60	23.80
Froude number $\mathbf{F_n}$ $[-]$		1.22	1.47	1.67	1.98	2.20	2.44	2.69
Averaged Courant number [-]	M1	120.06	121.37	122.11	123.44	124.49	124.47	124.92
	M2	119.95	121.28	122.34	123.66	123.79	124.62	125.16
	M3	120.03	121.31	122.40	123.74	123.89	124.70	125.14
	M4	120.10	121.25	122.25	123.70	123.78	124.68	124.67

Table 4: Averaged Y+

5. Free surface elevations

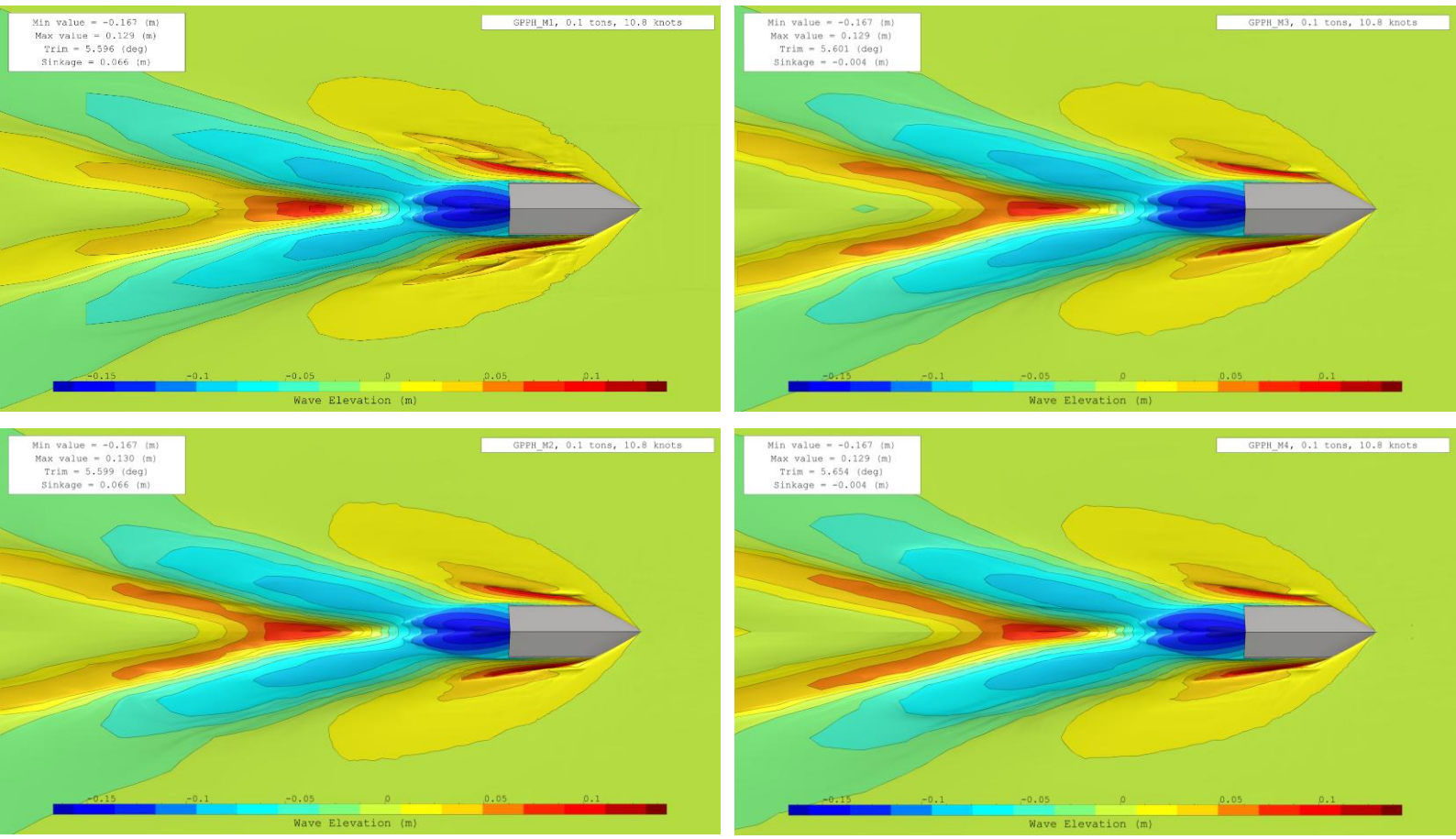

Figure 16: Free surface evolution at 10.80 knots

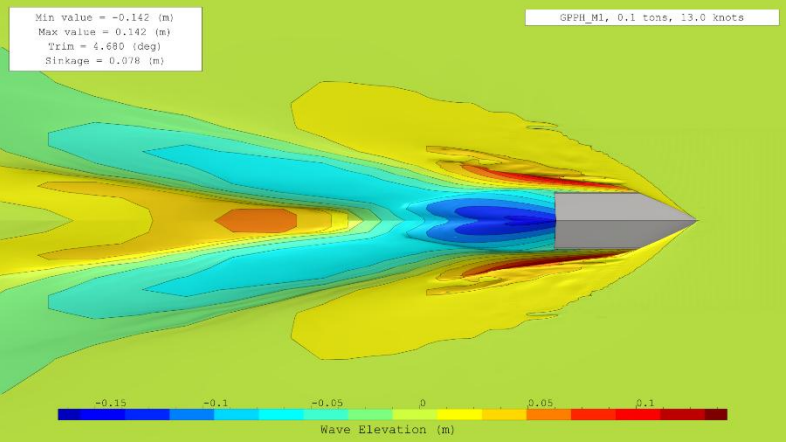

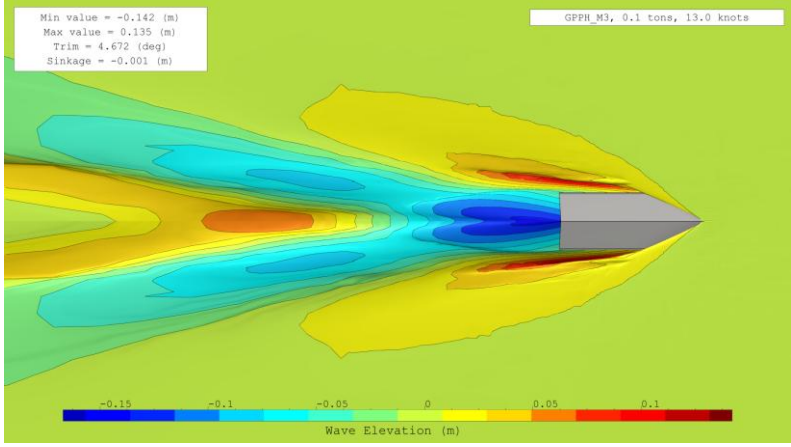

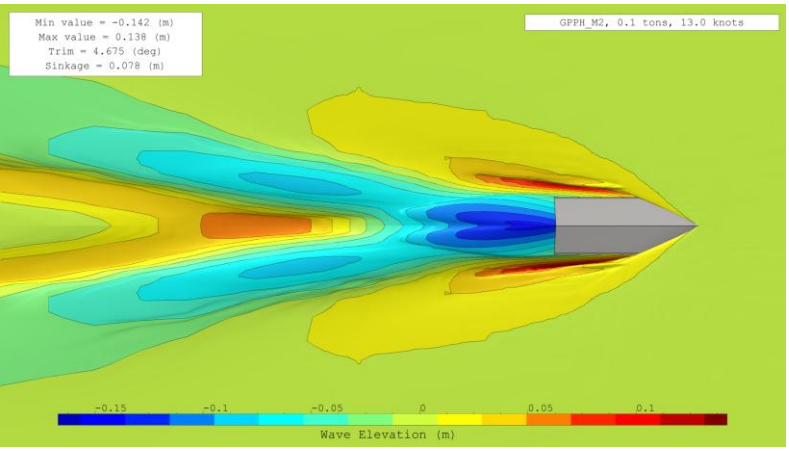

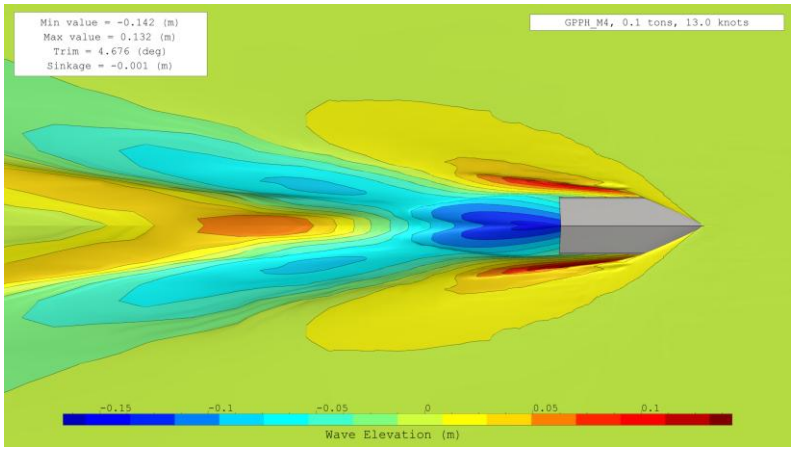

Figure 17: Free surface evolution at 13.00 knots

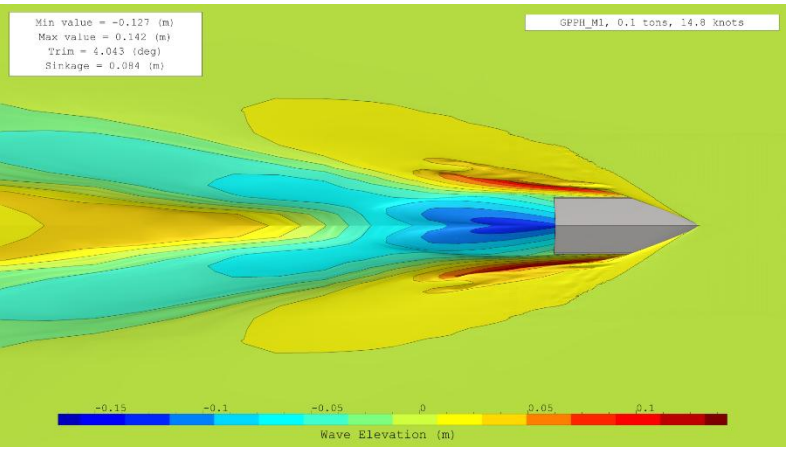

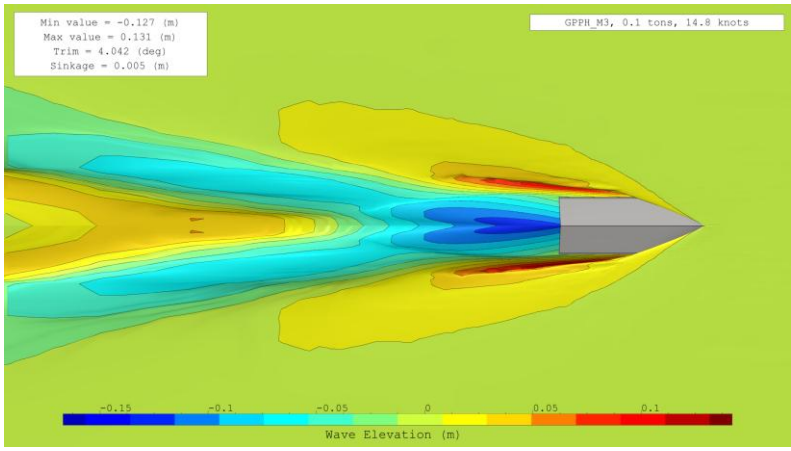

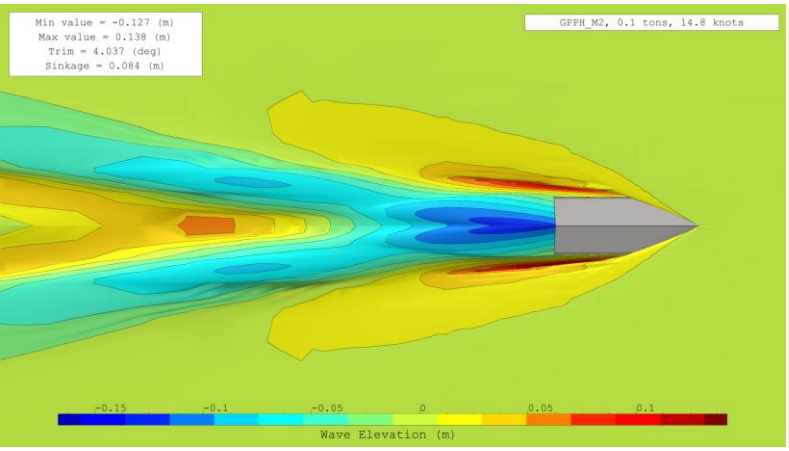

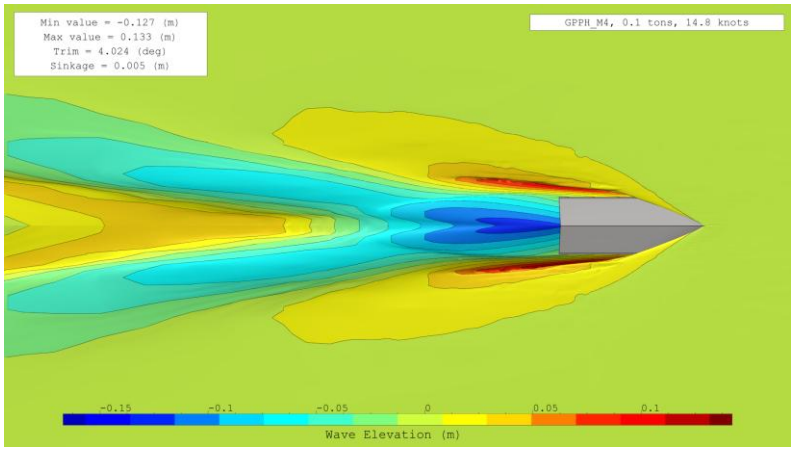

Figure 18: Free surface evolution at 14.80 knots

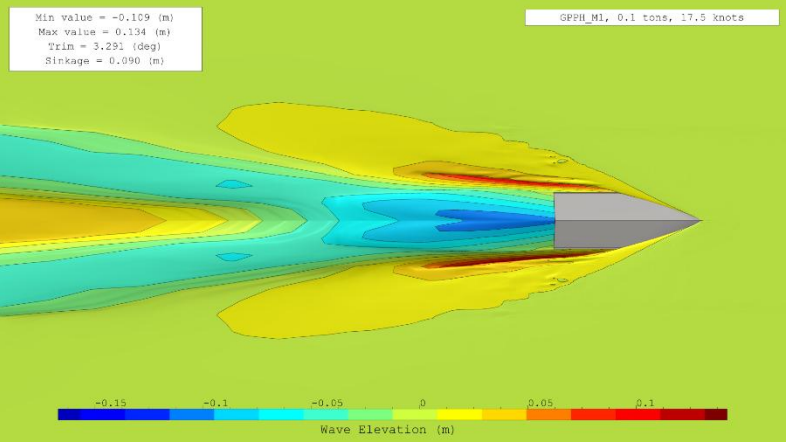

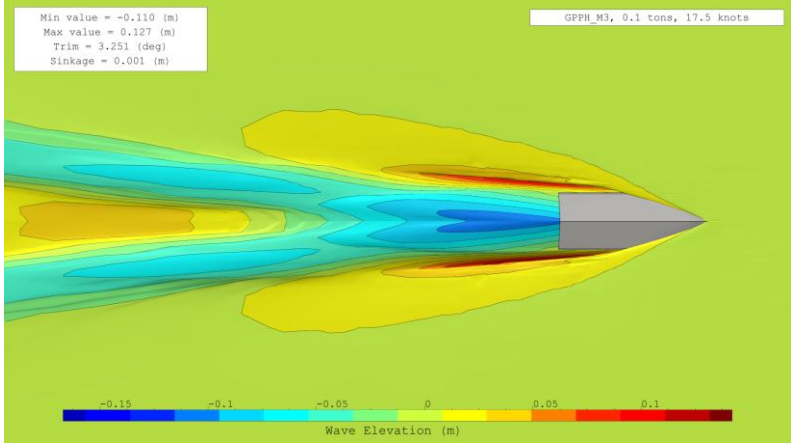

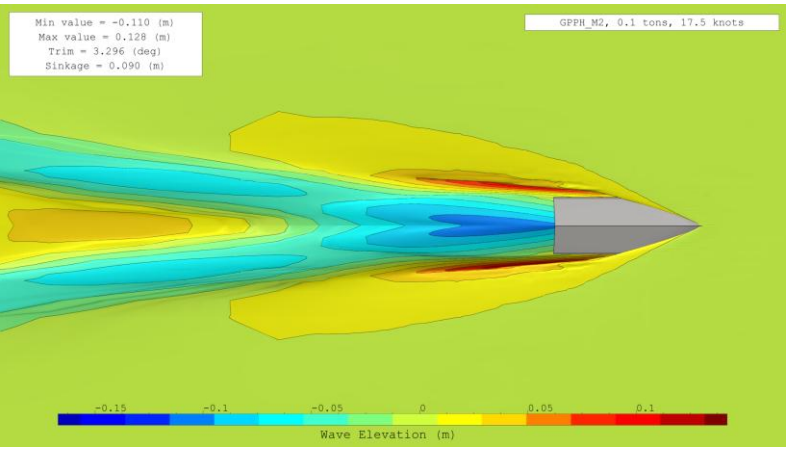

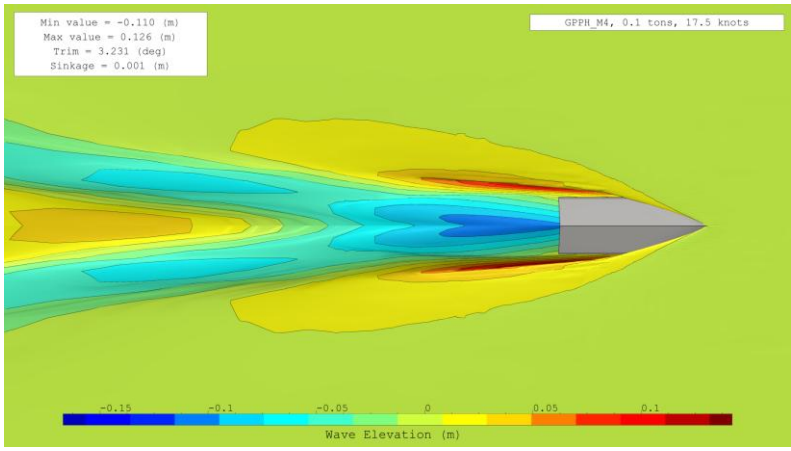

Figure 20: Free surface evolution at 17.50 knots

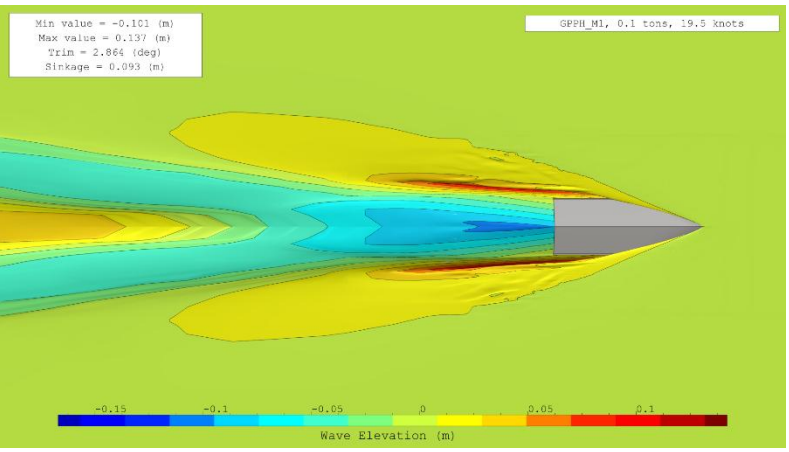

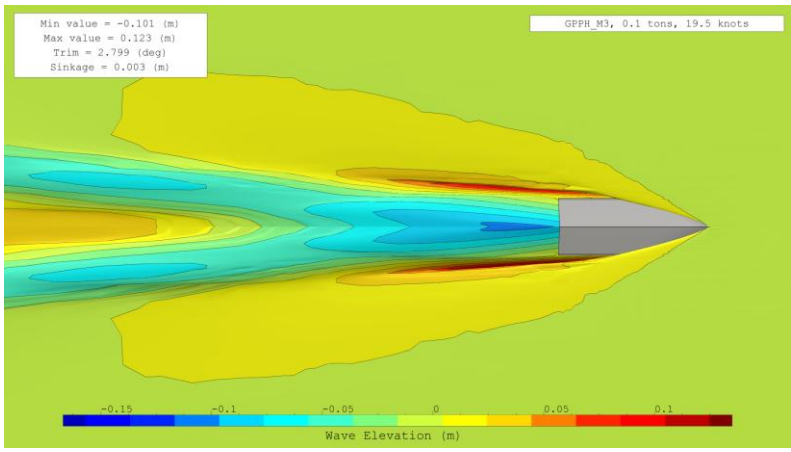

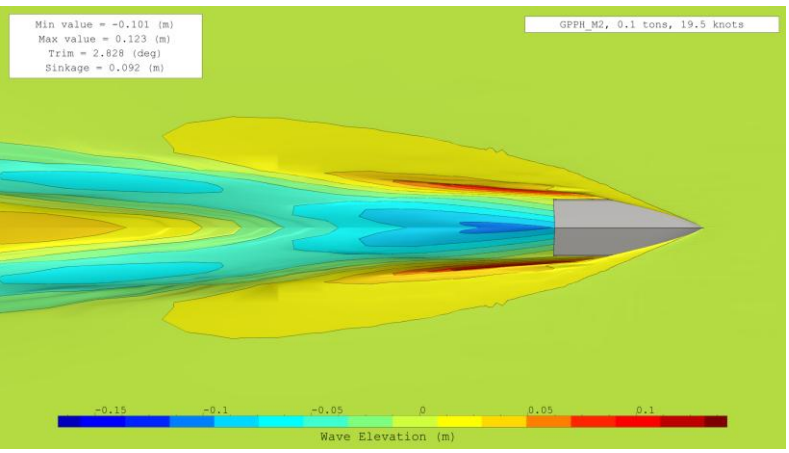

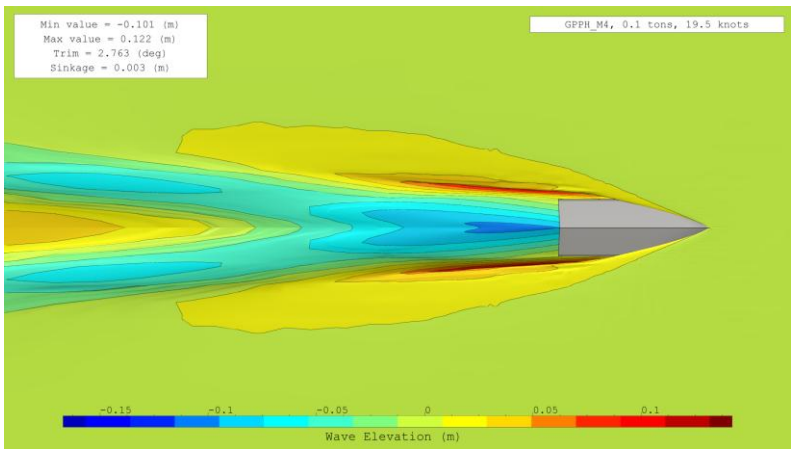

Figure 19: Free surface evolution at 19.50 knots

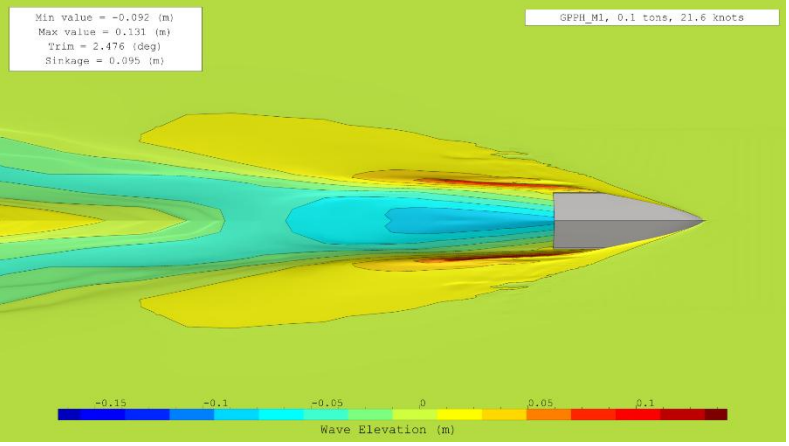

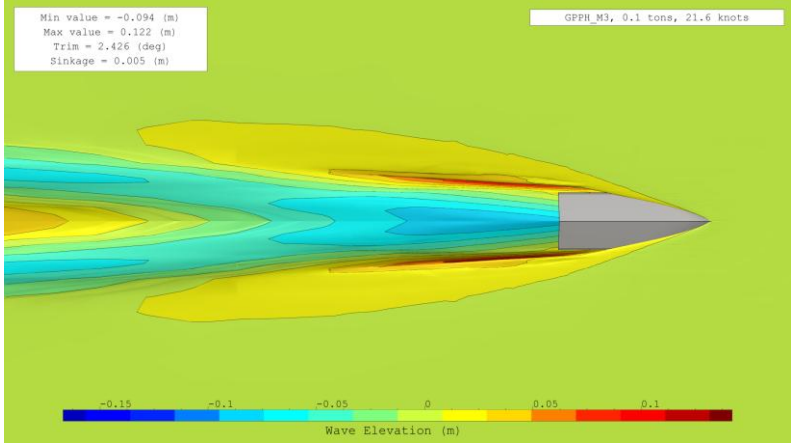

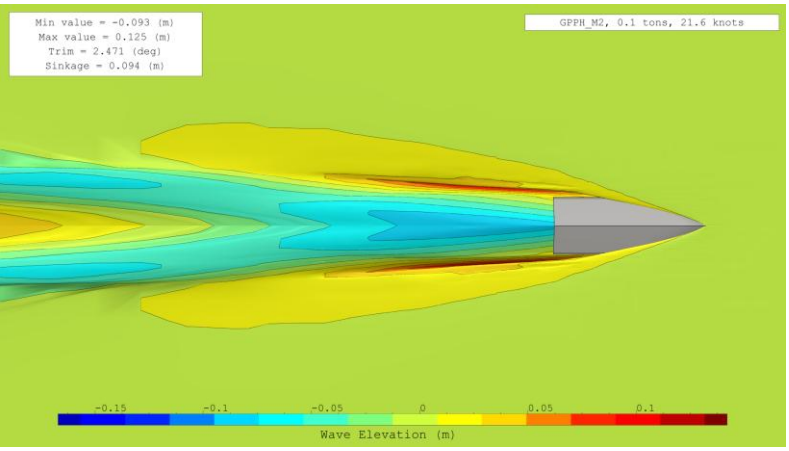

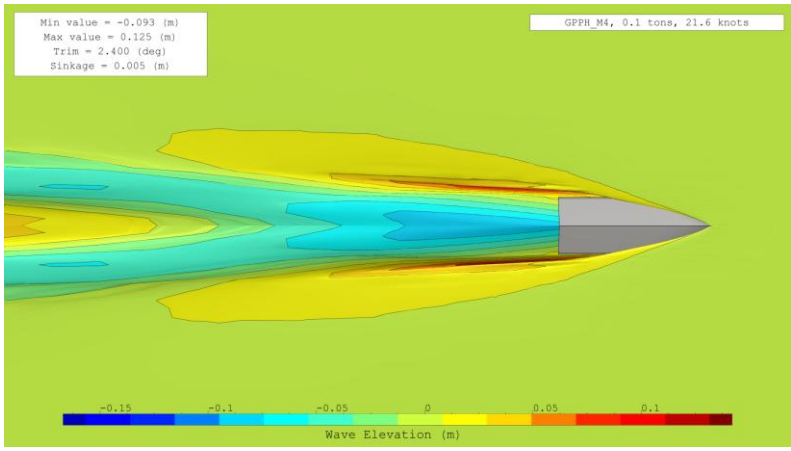

Figure 22: Free surface evolution at 21.60 knots

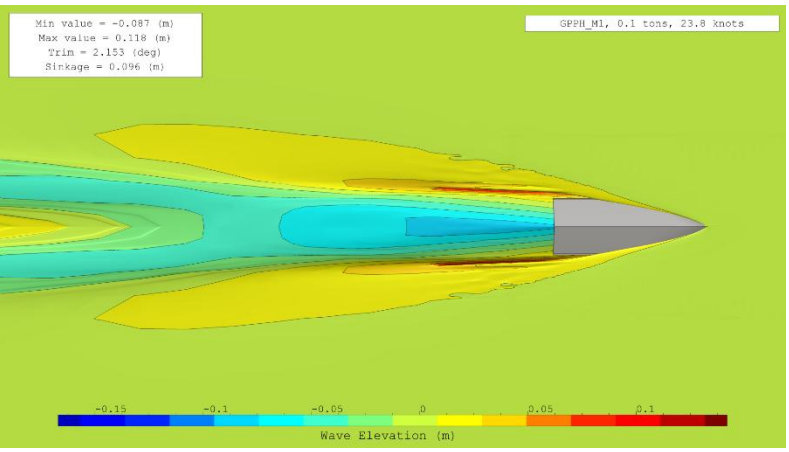

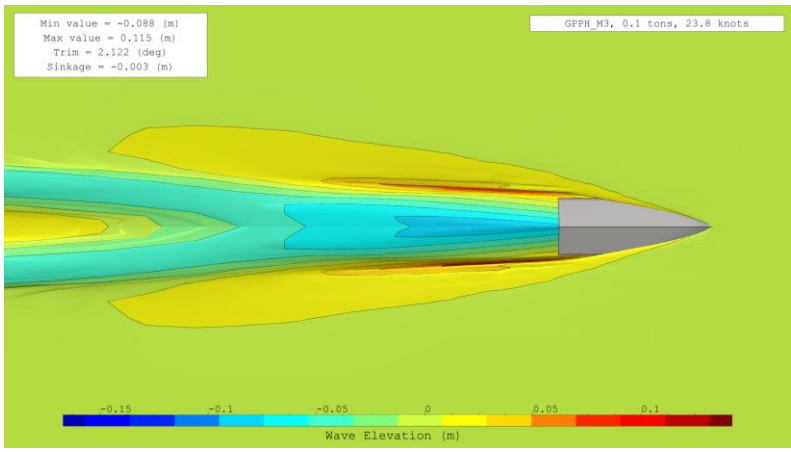

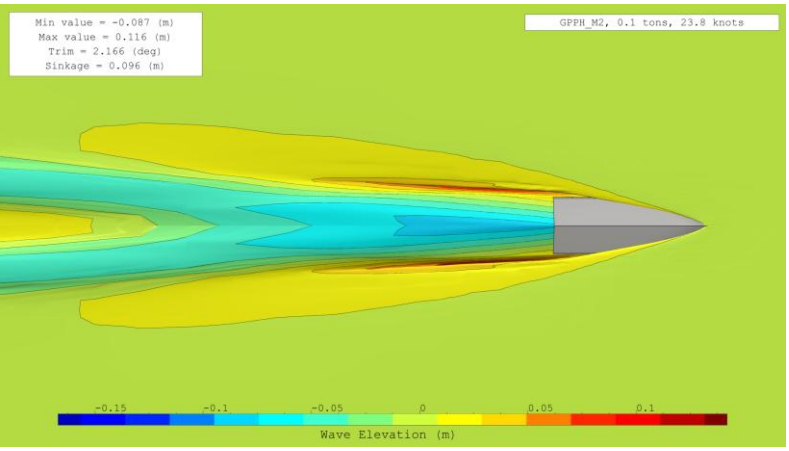

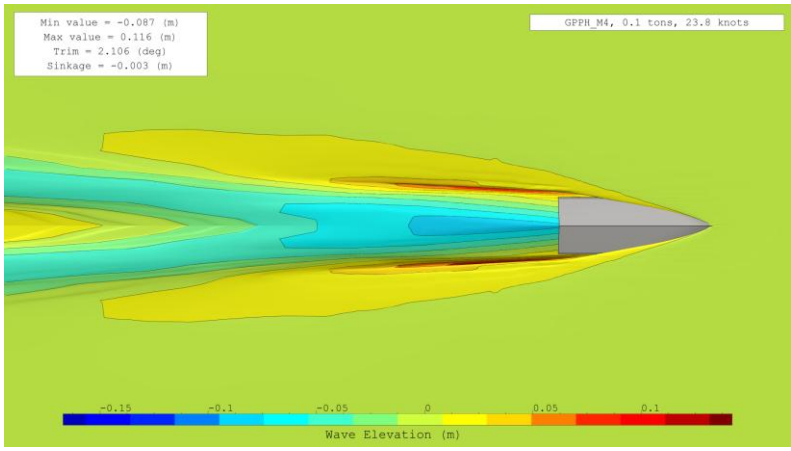

Figure 21: Free surface evolution at 23.80 knots

6. Comparison

a. Resistance

Figure 23 illustrates the progression of the GPPH resistance across different advance speeds in the top graph and table for each method. The middle table shows the absolute differences between CFD and EFD in Newtons, while the bottom table displays the relative difference between CFD and EFD as a percentage:

$$E\% = \frac{GPPH\_Mi - GPPH\_EFD}{GPPH\_EFD} * 100$$

We can observe that the CFD/EFD discrepancies are all the same order of magnitude. This indicates that all four methods effectively and accurately predict the resistance of the GPPH planning hull and can be used reliably.

Additionally, a slight difference can be noted with method M2, which is marginally more precise across all speeds in the study. This suggests that it is more appropriate to allow the ISIS-CFD solver from the Fidelity Fine Marine suite to freely resolve the dynamic sinkage without an initially pre-estimated value.

	Speed [knots]	Froude number [-]	● GPPH_M1	■ GPPH_M2	▲ GPPH_M3	★ GPPH_M4	+ GPPH_EFD
0	10.80	1.22	155.87	156.33	156.18	157.10	161.42
1	13.00	1.47	155.03	155.16	154.76	154.17	159.56
2	14.80	1.67	160.25	161.00	159.89	159.07	165.38
3	17.50	1.98	177.69	179.20	177.48	177.49	184.42
4	19.50	2.20	198.18	202.50	198.99	199.57	206.80
5	21.60	2.44	225.95	229.38	226.17	227.24	234.91
6	23.80	2.69	258.63	262.41	259.66	260.69	269.83

	Speed [knots]	Froude number [-]	X_0 = GPPH_M1, [N]	X_1 = GPPH_M2, [N]	X_2 = GPPH_M3, [N]	X_3 = GPPH_M4, [N]
0	10.80	1.22	-5.55	-5.09	-5.24	-4.32
1	13.00	1.47	-4.53	-4.40	-4.80	-5.39
2	14.80	1.67	-5.13	-4.38	-5.49	-6.31
3	17.50	1.98	-6.73	-5.22	-6.94	-6.93
4	19.50	2.20	-8.62	-4.30	-7.81	-7.23
5	21.60	2.44	-8.96	-5.53	-8.74	-7.67
6	23.80	2.69	-11.20	-7.42	-10.17	-9.14

	Speed [knots]	Froude number [-]	X_0 = GPPH_M1, [%]	X_1 = GPPH_M2, [%]	X_2 = GPPH_M3, [%]	X_3 = GPPH_M4, [%]
0	10.80	1.22	-3.44	-3.15	-3.25	-2.68
1	13.00	1.47	-2.84	-2.76	-3.01	-3.38
2	14.80	1.67	-3.10	-2.65	-3.32	-3.82
3	17.50	1.98	-3.65	-2.83	-3.76	-3.76
4	19.50	2.20	-4.17	-2.08	-3.78	-3.50
5	21.60	2.44	-3.81	-2.35	-3.72	-3.27
6	23.80	2.69	-4.15	-2.75	-3.77	-3.39

Figure 23: Comparison of total resistance

b. Pitch

Figure 24 illustrates the progression of the GPPH dynamic pitch response across different advance speeds in the top graph and table for each method. The middle table shows the absolute differences between CFD and EFD in degrees, while the bottom table displays the relative difference between CFD and EFD as a percentage:

$$E\% = \frac{GPPH\_Mi - GPPH\_EFD}{GPPH\_EFD} * 100$$

We can observe that the CFD/EFD discrepancies are all the same order of magnitude. This indicates that all four methods effectively and accurately predict the dynamic pitch attitude of the GPPH planning hull and can be used reliably.

Methods 1 and 2 appear to be the most precise, but overall, the discrepancies remain very small.

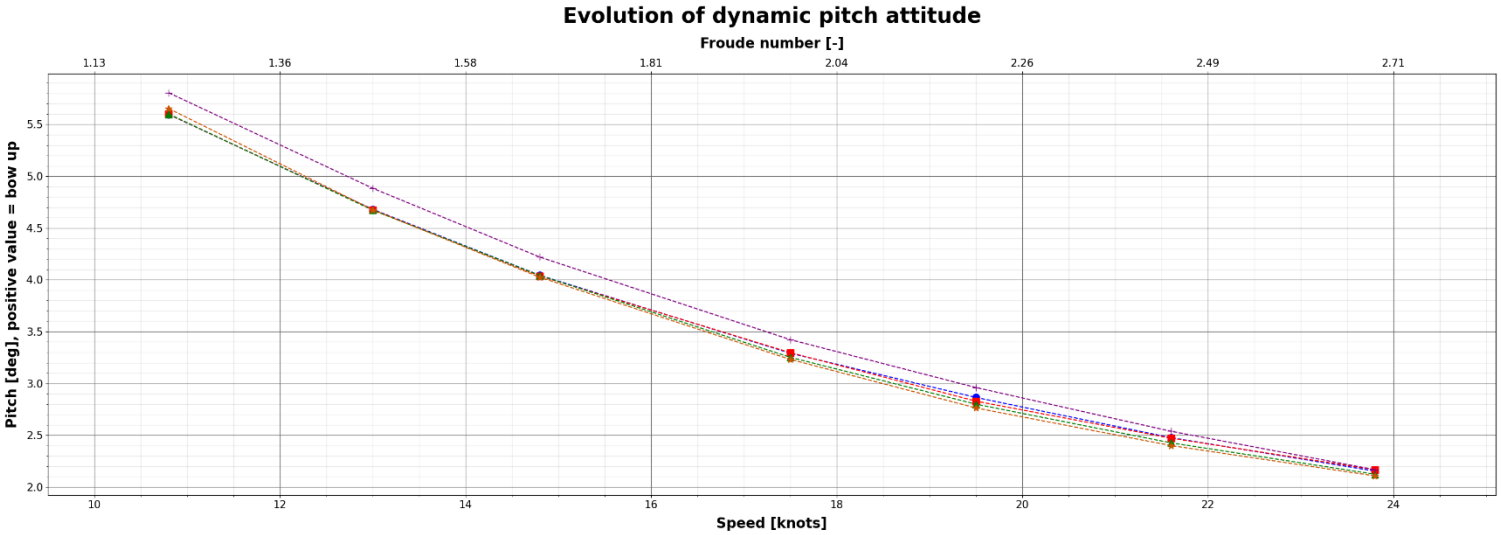

	Speed [knots]	Froude number [-]	● GPPH_M1	■ GPPH_M2	▲ GPPH_M3	★ GPPH_M4	+ GPPH_EFD
0	10.80	1.22	5.5964	5.5986	5.6011	5.6535	5.8054
1	13.00	1.47	4.6798	4.6753	4.6716	4.6758	4.8832
2	14.80	1.67	4.0433	4.0365	4.0424	4.0244	4.2191
3	17.50	1.98	3.2908	3.2963	3.2511	3.2312	3.4218
4	19.50	2.20	2.8638	2.8282	2.7988	2.7627	2.9597
5	21.60	2.44	2.4761	2.4712	2.4260	2.3998	2.5376
6	23.80	2.69	2.1530	2.1660	2.1224	2.1065	2.1666

	Speed [knots]	Froude number [-]	X_0 = GPPH_M1, [deg]	X_1 = GPPH_M2, [deg]	X_2 = GPPH_M3, [deg]	X_3 = GPPH_M4, [deg]
0	10.80	1.22	-0.209	-0.207	-0.204	-0.152
1	13.00	1.47	-0.203	-0.208	-0.212	-0.207
2	14.80	1.67	-0.176	-0.183	-0.177	-0.195
3	17.50	1.98	-0.131	-0.126	-0.171	-0.191
4	19.50	2.20	-0.096	-0.132	-0.161	-0.197
5	21.60	2.44	-0.061	-0.066	-0.112	-0.138
6	23.80	2.69	-0.014	-0.001	-0.044	-0.060

	Speed [knots]	Froude number [-]	X_0 = GPPH_M1, [%]	X_1 = GPPH_M2, [%]	X_2 = GPPH_M3, [%]	X_3 = GPPH_M4, [%]
0	10.80	1.22	-3.60	-3.56	-3.52	-2.62
1	13.00	1.47	-4.17	-4.26	-4.33	-4.25
2	14.80	1.67	-4.17	-4.33	-4.19	-4.61
3	17.50	1.98	-3.83	-3.67	-4.99	-5.57
4	19.50	2.20	-3.24	-4.44	-5.44	-6.66
5	21.60	2.44	-2.42	-2.62	-4.40	-5.43
6	23.80	2.69	-0.63	-0.03	-2.04	-2.77

Figure 24: Comparison of dynamic pitch attitude

c. Heave

Figure 25 illustrates the progression of the GPPH dynamic heave response across different advance speeds in the top graph and table for each method. The middle table shows the absolute differences between CFD and EFD in meters, while the bottom table displays the relative difference between CFD and EFD as a percentage:

$$E\% = \frac{GPPH\_Mi - GPPH\_EFD}{GPPH\_EFD} * 100$$

We can observe that the CFD/EFD discrepancies are all the same order of magnitude. This indicates that all four methods effectively and accurately predict the dynamic heave attitude of the GPPH planning hull and can be used reliably.

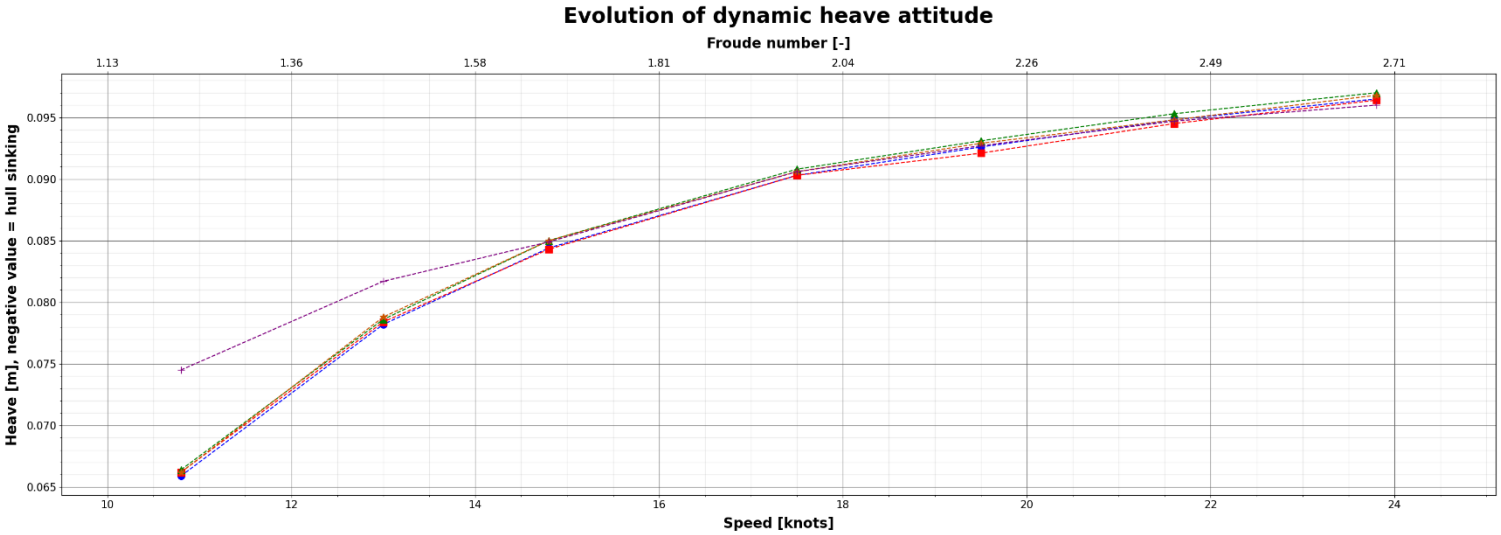

	Speed [knots]	Froude number [-]	● GPPH_M1	■ GPPH_M2	▲ GPPH_M3	★ GPPH_M4	+ GPPH_EFD
0	10.80	1.22	0.0659	0.0662	0.0664	0.0662	0.0745
1	13.00	1.47	0.0782	0.0784	0.0786	0.0788	0.0817
2	14.80	1.67	0.0844	0.0843	0.0850	0.0850	0.0849
3	17.50	1.98	0.0903	0.0903	0.0908	0.0906	0.0906
4	19.50	2.20	0.0926	0.0921	0.0931	0.0929	0.0927
5	21.60	2.44	0.0948	0.0945	0.0953	0.0948	0.0947
6	23.80	2.69	0.0965	0.0964	0.0970	0.0968	0.0960

	Speed [knots]	Froude number [-]	X_0 = GPPH_M1, [m]	X_1 = GPPH_M2, [m]	X_2 = GPPH_M3, [m]	X_3 = GPPH_M4, [m]
0	10.80	1.22	-0.009	-0.008	-0.008	-0.008
1	13.00	1.47	-0.003	-0.003	-0.003	-0.003
2	14.80	1.67	-0.001	-0.001	0.000	0.000
3	17.50	1.98	-0.000	-0.000	0.000	0.000
4	19.50	2.20	-0.000	-0.001	0.000	0.000
5	21.60	2.44	0.000	-0.000	0.001	0.000
6	23.80	2.69	0.001	0.000	0.001	0.001

	Speed [knots]	Froude number [-]	X_0 = GPPH_M1, [%]	X_1 = GPPH_M2, [%]	X_2 = GPPH_M3, [%]	X_3 = GPPH_M4, [%]
0	10.80	1.22	-11.54	-11.14	-10.87	-11.14
1	13.00	1.47	-4.28	-4.04	-3.79	-3.55
2	14.80	1.67	-0.59	-0.71	0.12	0.12
3	17.50	1.98	-0.33	-0.33	0.22	0.00
4	19.50	2.20	-0.11	-0.65	0.43	0.22
5	21.60	2.44	0.11	-0.21	0.63	0.11
6	23.80	2.69	0.52	0.42	1.04	0.83

Figure 25: Comparison of dynamic heave attitude

d. Simulation time

Figure 26 compares the computation times in hours for each method. Since simulations are run on an optimal number of cores determined by the mesh cell count, it is essential to consider the number of cores utilized when analysing performance.

The simulation time for the entire resistance curves are:

- M1: 114.01 hours
- M2: 47.78 hours
- M3: 44.91 hours
- M4: 24.67 hours

It can be observed that, method by method, the simulation time decreases, ultimately reaching a duration between 3 and 4 hours. This is remarkable, as it represents a reduction of approximately 4.4 to 4.9 times the initial simulation time. It is also important to note that our initial method (M1) was already an optimized version compared to common practice, where a pre-estimated pitch angle is typically not considered. This means that the actual reduction in computation time would be even more significant when compared to standard approaches.

The mesh deformation approach (transition from M1 to M2) and the removal of the acceleration ramp (transition from M3 to M4) are the two most effective modelling strategies for reducing computation time.

	Speed [knots]	Froude number [-]	● Core [-]	● GPPH_M1	■ Core [-]	■ GPPH_M2	▲ Core [-]	▲ GPPH_M3	★ Core [-]	★ GPPH_M4
0	10.80	1.22	32	16.68	24	6.63	24	5.87	24	3.53
1	13.00	1.47	32	18.00	24	6.48	24	5.80	24	3.68
2	14.80	1.67	32	15.92	26	6.80	26	6.58	26	3.43
3	17.50	1.98	32	15.48	26	6.67	26	6.25	26	3.40
4	19.50	2.20	32	15.78	26	6.93	26	6.70	26	3.58
5	21.60	2.44	32	16.25	26	7.00	26	6.73	26	3.43
6	23.80	2.69	32	15.90	26	7.27	26	6.98	26	3.62

Figure 26: Computational time in hours

7. Conclusion

This study investigates the influence of meshing strategies and numerical parameters on the simulation accuracy and computational efficiency of planning hull hydrodynamics using CFD. The comparison between different methods reveals that all tested approaches provide reliable predictions for resistance, dynamic pitch, and dynamic heave, with discrepancies relative to experimental data remaining within the same order of magnitude.

For resistance predictions, method M2 stands out as the most precise across all speeds, making it the preferred choice when accuracy is the priority. Similarly, M1 and M2 provide the best results for dynamic pitch, while all methods perform similarly for dynamic heave. However, when fast turnaround times are required, such as for design space exploration, method M4 offers a significantly reduced computational cost with only a slight loss in accuracy.

Beyond accuracy, computational efficiency is a critical factor in simulation performance. The study highlights a significant reduction in computation time, ultimately reaching a duration between 3 and 4 hours. Approximately 4.4 to 4.9 times faster than the initial simulation setup. Given that method M1 was already optimized compared to standard practices, the actual time savings are even more substantial. The most effective strategies for improving computational performance are the implementation of a mesh deformation approach and the removal of the acceleration ramp.

Overall, this study demonstrates that careful selection of meshing strategies and numerical parameters can achieve both high accuracy and computational efficiency in CFD simulations of planning hulls. Method M2 emerges as a strong candidate for future simulations, striking an optimal balance between precision and reduced computational cost.

Despite these optimizations, the overset method remains a valuable tool. An inaccurately pre-estimated equilibrium state that deviates too far from the dynamic one can lead to simulation instabilities in methods M2, M3, and M4. Therefore, validating all four methods was essential to ensure adaptability to different project requirements.

All these best practices and methodological improvements have been integrated into NepTech's digital towing tank, ensuring high-fidelity simulations tailored to the specific needs of naval architecture and hydrodynamic design.

Bibliography

Lee, E., R. Weil, C., & Fullerton, A. (2017). *Experimental Results for the Calm Water Resistance of the Generic Prismatic Planing Hull (GPPH).* West Bethesda: Naval Surface Warfare Center Carderock Division.